Green Energy and Fuel Research

Article

Synergistic and Antagonistic Effects of Catalytic Torrefaction-Pyrolysis of Woody Biomass in a Carbon Dioxide Atmosphere for Biofuel Production

Elizabeth Wanchisn Smith [1], Ria Aniza [2,3,4], Anelie Petrissans [2,*], Rafael Lopes Quirino [1,*], Baptiste Colin [2], Mathieu Petrissans [2], and Wei-Hsin Chen [5,6,7]

[1] Biochemistry, Chemistry and Physics Department, Georgia Southern University, Statesboro, GA 30460, USA
[2] Université de Lorraine, INRAE, LERMAB, F-88000 Epinal, France
[3] International Doctoral Degree Program in Energy Engineering, National Cheng Kung University, Tainan 701, Taiwan
[4] Department of Environmental Engineering, Institut Teknologi Sepuluh Nopember, Surabaya 60111, Indonesia
[5] Department of Aeronautics and Astronautics, National Cheng Kung University, Tainan 701, Taiwan
[6] Research Center for Smart Sustainable Circular Economy, Tunghai University, Taichung 407, Taiwan
[7] Department of Mechanical Engineering, National Chin-Yi University of Technology, Taichung 411, Taiwan
* Correspondence: anelie.petrissans@univ-lorraine.fr (A.P.); rquirino@georgiasouthern.edu (R.L.Q.)
Received: 1 April 2025; Revised: 27 May 2025; Accepted: 13 June 2025; Published: 19 June 2025

Abstract: Torrefaction-pyrolysis is the thermal treatment of biomass in an inert atmosphere between 105 °C and 800 °C to break carbon bonds and produce biofuels. The purpose of this study is to examine how woody biomass with different particle sizes (250 µm and 500 µm), wood types (Poplar and Fir), and catalyst types (K, Na, and Mg) responds to catalytic thermochemical conversion in a CO_2 environment. Torrefaction-pyrolysis of woody biomass shows the Boudouard equilibrium responds after 780 °C for K and Na-catalysts, except in samples impregnated with Mg-catalyst. When K-catalyst material is present, the C-O-C signal regarding the glycosidic linkages from cellulose and hemicelluloses in Fir is observed to decrease the most. This is related to the fact that Fir (22.43 wt.%) has nearly twice as many hemicelluloses as Poplar (12.18 wt.%), making it less thermally stable and more vulnerable to the prolonged drying required following catalyst impregnation.

Keywords: torrefaction; pyrolysis; catalytic reaction; CO_2 carrier gas; Boudouard equilibrium

1. Introduction

Carbon dioxide emissions reached 149% of pre-industrial levels while methane and nitrous oxide emissions reached 262% and 124%, respectively, in 2021 [1]. Thus, distinctive solutions are necessary to reduce GHG excessive production by changing the focus away from reliance on non-renewable fossil fuels and toward renewable, clean, and sustainable energy. Converting biomass to biofuel is a low-cost, competitive alternative to fossil fuels due to its carbon neutrality and availability [2–4]. Biomass, such as wood waste from the timber industry, is a prospective candidate for biomass-based renewable energy, with 95.1 million tons of dead biomass generated in the state of California alone between the years 2012 to 2017 [5]. Currently, the primary means of disposal is through mass burning, releasing carbon dioxide, particulate matter, and other pollutants into the atmosphere [6,7]. Utilizing woody biomass as a sustainable fuel source provides a practical way to get rid of these dead standing trees and use them as feedstock for making biofuel [8,9] in addition to woody furniture, building structures, and bio-composite [10–12].

Biomass is also a carbon-neutral fuel source since the amount of carbon emitted is equivalent to the amount captured during growth [13,14]. The energy from the conversion of sunlight and carbon dioxide during photosynthesis is stored in the carbon-carbon bonds found within the three main biopolymers of biomass [15]. Figure 1 is the illustration of the chemical structure of three biopolymers in wood. Cellulose is composed of a linear polymer chain of glucose monomers held tightly together by hydrogen bonding [9]. Lignin is composed of three main phenolic units organized randomly, resulting in variable structures serving to hold the material together [13]. Hemicelluloses are composed of short polysaccharide chains. Xylan is an example of a hemicellulose [16,17]. A thorough understanding of the chemical processes involved in breaking these bonds can lead to the efficient extraction of the energy in biomass. However, woody biomasses have high moisture content and heterogeneity in addition to low bulk energy density, and low uniformity across different species, limiting their efficiency of conversion to biofuels when undergoing torrefaction-pyrolysis [17,18].

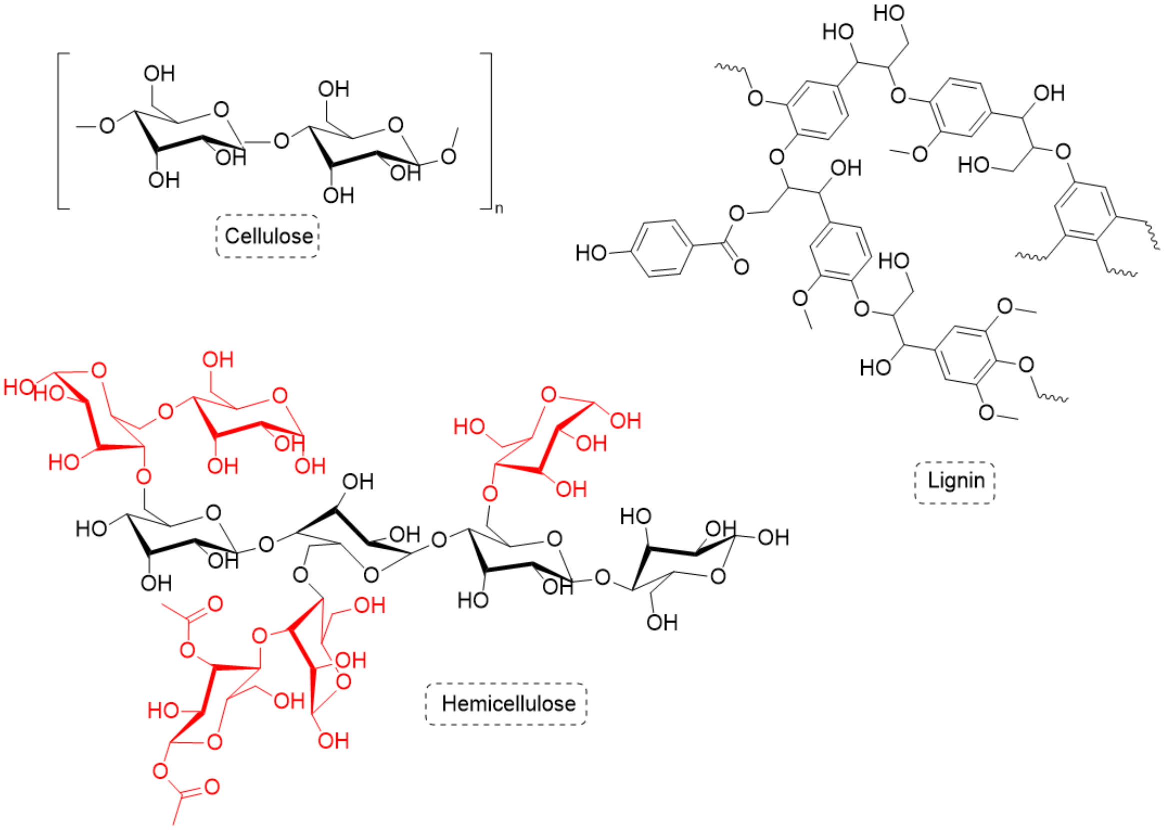

Figure 1. Three main biopolymers of woody biomass: cellulose, an example of hemicelluloses, and an example of lignin.

Torrefaction heats biomass between 200 °C and 350 °C, improving its energy potential and reducing greenhouse gases by 85% compared to coal [2,19,20]. Pyrolysis, above 350 °C, produces liquid and gas products through extensive degradation [13,14,21]. Catalysts like potassium (K), sodium (Na), and magnesium (Mg) enhance both processes [22,23]. Potassium carbonate, for example, reduces torrefaction time by 67%, increases heating value, and improves gas yields [24,25]. NaCl boosts pyrolysis yield and heating value [26], while $MgCl_2$ lowers pyrolysis temperature and increases yield in cabbage-based biochar [27]. MgO, however, shows low activity for sugar cane pyrolysis [28]. Additionally, the inert carrier gas in torrefaction-pyrolysis, such as CO_2 atmosphere, differs from N_2 due to CO_2's vibrational modes and electrophilic structure, allowing it to absorb more radiation and be more reactive [29]. This reactivity supports the Boudouard equilibrium, where solid carbon reacts with CO_2 to form CO above 700 °C. Studies have shown increased CO, H_2, and CH_4 production at these temperatures, influenced by heating rate [30–32]. Guizani et al. [33] found that adding 20–40% CO_2 to N_2 during pyrolysis of hardwood beech species increased mass loss by 10–13%, enhanced gas yields, and produced more carbon-rich char by altering hydrogen and oxygen interactions.

Limited studies have explored torrefaction-pyrolysis in pure CO_2, especially with woody biomass. Most research on catalysis in CO_2 has focused on expensive heavy metals (Pd, Pt, Ni), leaving earth metal catalysis in CO_2 of interest. To address the challenge, thus, this study aims to examine the effects of CO_2 on the torrefaction-pyrolysis of hard (Poplar) and soft (Fir) woods with different particle sizes (250 µm and 500 µm) and three catalysts (KCl, NaCl, $MgCl_2$) using various analytical methods. The novel approach combines torrefaction and pyrolysis in one protocol to provide a comprehensive understanding of how CO_2 influences both processes.

2. Materials and Methods

2.1. Materials

The wood samples were obtained from a local timber in the Grand Est area (France). The selected wood species for this study were Fir wood (*Abies pectinata*), and Poplar wood (*Populus nigra*) as they are all common waste woods in the Vosges region in France. The woods were ground using a knife-mill SM100 (Retsch, Germany) equipped with trapezoidal meshes of 0.5 mm. The wood powder was sieved using meshes to obtain particle sizes of 250 µm and 500 µm. All wood samples were dried at 103 °C overnight prior to catalyst impregnation. Potassium chloride (KCl—99.5%) and sodium Chloride (NaCl—99.9%) were delivered by VWR. Meanwhile, crystalline anhydrous magnesium chloride ($MgCl_2$—99.0%) was obtained from Alfa Aesar.

2.2. Methods

2.2.1. Catalyst Impregnation

According to a procedure commonly adopted in the literature, earth metals were inserted into the biomass through chemical impregnation using KCl, NaCl, and $MgCl_2$ [34]. The catalytic impregnation solutions were prepared by dissolving KCl, $MgCl_2$, and NaCl with deionized water in three different concentrations 0.025 ± 0.005, 0.05 ± 0.004, and 0.1 M. Research has indicated that 0.025 M of catalyst could efficiently catalyze the transformation of furfurals produced from biomass into useful compounds such as cyclopentanone [35,36], 0.05 M improved accessibility to the acid site and mass diffusion [37], meanwhile, the concentration higher than 0.1 M might revealed negative consequences caused by char pore clogging [38]. Dry Fir and Poplar samples of 250 µm and 500 µm were impregnated with three types of catalyst. The samples were impregnated by mixing 3.0 g of oven-dried wood samples with 250 mL of salt solution. The mixture was stirred for 1 h at ambient conditions before undergoing vacuum filtration. Each sample was then placed in an oven at 103 °C until the weight was stable.

2.2.2. TGA Experiments

The behavior of impregnated and raw wood during torrefaction-pyrolysis was analyzed by thermogravimetric analysis using a simultaneous thermal analyzer (TGA/DSC-STA 449 F3 Jupiter, Netzsch, Selb, Germany) with a CO_2 flow of 50 mL/min. Oven-dried powder samples of approximately 10.0 mg were loaded in a ceramic crucible and heated from room temperature to 105 °C under a CO_2 atmosphere. That temperature was maintained for 10 min to remove residual moisture. Each sample was then heated to 350 °C at a heating rate of 20 $°C \cdot min^{-1}$. The temperature was maintained at 350 °C for 30 min to observe torrefaction conditions. After that, the temperature was increased to 800 °C at a heating rate of 20 $°C \cdot min^{-1}$ and maintained at 800 °C for 30 min in a pyrolysis step. Finally, the atmosphere was switched to air, and the sample was kept at 800 °C for an additional 30 min for a complete combustion of all organic residue. The curve of solid weight percentage as a function of temperature was obtained (TG), and the derivative of the TG (DTG) as a function of time was considered. The TGA experiments were duplicated, and the average curves are presented herein. All the results of TGA experiments were controlled with the $\alpha \leq 0.1$ (maximum 10% error).

2.2.3. SEM and FTIR Tests

Each wood type was characterized by its fiber composition, surface morphology/topography, and chemical functional group by fiber analysis, SEM, and FTIR spectroscopy, respectively. Fiber analysis was used to determine the composition of hemicelluloses, cellulose, and lignin in lignocellulosic biomass materials [8,39]. A Whatman 41, circular, ashless filter paper with a 42.5 mm diameter was used. For SEM, approximately 2.0 mg of samples were placed on copper tape and mounted onto a JEOL Aluminum Specimen Mount (9.5 mm × 9.5 mm) from TED PELLA, INC. The mounted sample was coated in platinum using a Denton Vacuum Desk V Sputter and dried in a vacuum desiccator for 4 days before being imaged with a JEOL JSM-7600F Scanning Electron Microscope equipped with an Energy Dispersive X-ray (EDX) detector. EDX spectroscopy was used to determine the elemental composition of each sample. Furthermore, approximately 0.05 g of each sample was used for FTIR spectroscopy using a Thermo Scientific Nicolet iS10 FTIR spectrometer (Madison, WI, USA) equipped with an attenuated total reflectance (ATR) accessory. All spectra were normalized based on the H-C (sp^3) signal at ~2900 cm^{-1} in each spectrum. All the results of EDX experiments were controlled with the $\alpha \leq 0.1$ (maximum 10% error).

3. Results and Discussion

3.1. Characterization of Woody Sample

Fir (softwood) and Poplar (hardwood) are the two most common wood species in France’s forests. In order to analyze the chemical composition within the raw sample of Fir and Poplar woods, some tests were performed, including fiber analysis and higher heating value (HHV) (Table 1). The Fir sample has a deep brownish color compared to the Poplar sample, which shows more light brownish. The fiber analysis shows Fir contains cellulose at 45.24 wt.%, lignin at 32.33 wt.%, and hemicelluloses at 22.43 wt.%, meanwhile, Poplar contains cellulose at 63.93 wt.%, lignin at 23.89 wt.%, and hemicelluloses at 12.18 wt.%. Hardwood (Poplar) typically has a higher cellulose content compared to softwood (Fir). Cellulose is a polymer that works to increase the strength, hardness, and durability of wood [5,16]. This is why hardwoods are naturally more durable and stronger than softwoods. In terms of energy content, the calorific value test of HHV indicates that Fir has approximately 9.65% more energy (19.88 MJ/kg) than Poplar (18.13 MJ/kg).

Table 1. Wood characterization of Fir and Poplar.

Procedure [a]	**Fir**	**Poplar**
Sample image		
Fiber Analysis (wt.%)		
Cellulose	45.24	63.93
Hemicelluloses	22.43	12.18
Lignin	32.33	23.89
HHV (MJ/kg)	19.88	18.13

a: The experiment was performed duplicate with an error margin α ≤ 10%.

In order to provide an overview of catalytic species retained after impregnation, selected samples with the same particle size (500 µm) were analyzed by SEM and EDX, as shown in Figure 2. A consistent magnification of 400× was adopted for imaging. The most notable information gained from SEM and EDX data includes the verification that impregnation was successful, as seen by the relative concentrations of K, Mg, Na, and Cl atoms in each of the impregnated samples analyzed. It can also be noted that in the areas examined, impregnation appears uniform based on the elemental mappings obtained. It is worth mentioning that the concentration of Cl retention in Poplar after impregnation with 0.1 M KCl is approximately twice as high as that of Fir impregnated with 0.05 M KCl, Poplar impregnated with 0.05 M NaCl, Poplar impregnated with 0.05 M $MgCl_2$, and approximately three times higher than raw Poplar. This indicates that the retention of Cl atoms from KCl and NaCl is directly dependent on the concentration of the impregnation solution, regardless of the wood. It is somewhat surprising that $MgCl_2$ didn't result in more retention of Cl atoms, as expected from its original composition.

It is important to highlight the significantly high concentration of K and Cl in raw Poplar and the complete absence of Mg and Na (Table 2). In fact, the lower K concentration in Poplar impregnated with 0.05 M NaCl and 0.05 M $MgCl_2$ with respect to the raw wood (Table 2) suggests that most of the Potassium naturally present in the wood leaches out during the impregnation process. The same effect is not observed with Cl.

FTIR was used to analyze samples before and after impregnation to determine if the impregnation process and the subsequent drying of impregnated samples at 103 °C for an extended time affected the composition of the woody biomass before torrefaction-pyrolysis. In Table 2, the ratios of C-O-C signals (~1100 cm^{-1}), pertaining to glycosidic bonds from cellulose and hemicelluloses, and OH signals (~3500 cm^{-1}) present in impregnated samples can be seen. It can be noted that while the changes in Poplar-impregnated samples are negligible, Fir seems more susceptible to the effect of drying in the presence of impregnated atoms. Indeed, there is a slight decrease in C-O-C relative to OH for all Fir-impregnated samples in comparison to the raw wood. It is possible that during drying, the extended exposure of the sample to an elevated temperature (103 °C) triggered the cleavage of some glycosidic bonds in the most thermally susceptible components, such as hemicelluloses.

The C-O-C bond vibration is only present in glycosidic bonds, which is the fundamental connection between sugar units to form polysaccharides, such as cellulose and hemicelluloses [40]. When a relative decrease in that signal is detected, it implies the rupture of the C-O-C connection. The decrease in C-O-C in Fir is largest in the presence of K (Table 2). The higher susceptibility of Fir to cleavage of glycosidic bonds can be correlated to its hemicellulose content. Fir has almost twice as many hemicelluloses (22.43 wt.%) as Poplar (12.18 wt.%), therefore, they are less thermally stable and more sensitive to the extended drying imposed after impregnation. The considerable difference in hemicellulose content can also be seen by the initial (C-O-C):(OH) ratios of Fir and Poplar (Table 2).

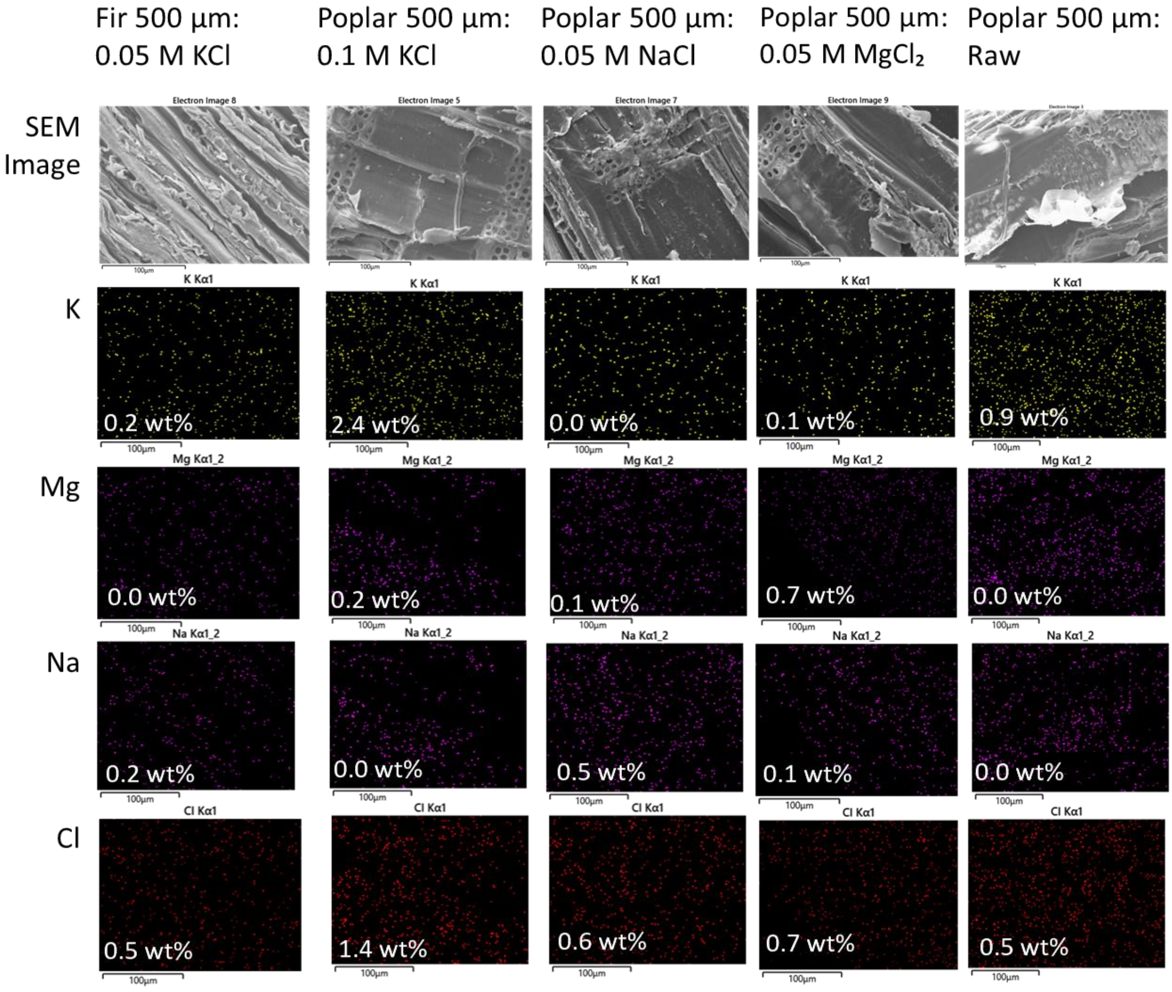

Figure 2. SEM and EDX results of selected samples.

Table 2. FTIR peak area results of Poplar and Fir impregnated samples.

Biomass	Normalized O-H Peak Area (a.u.)	Normalized C-O-C Peak Area (a.u.)	(C-O-C):(O-H) Peak Area Ratio
Fir (0.05 M)			
Fir Raw	7.54	16.92	2.24
Fir NaCl	9.78	20.17	2.06
Fir KCl	10.58	19.24	1.82
Fir $MgCl_2$	10.16	19.66	1.94
Poplar (0.05 M)			
Popar Raw	7.14	13.05	1.83
Poplar NaCl	8.63	15.16	1.76
Poplar KCl	10.08	19.65	1.95
Poplar $MgCl_2$	9.84	16.98	1.73

3.2. Thermogravimetric Analysis

TGA and DTG of Poplar and Fir raw samples were performed for two particle sizes (250 µm and 500 µm) in a CO_2 atmosphere. The results are presented in Figure 3. The thermodegradation of wood samples can be divided into two steps: torrefaction and pyrolysis. Torrefaction results in partial degradation of the wood polymers from 105 °C to 350 °C. Pyrolysis results in the extensive degradation of carbon-carbon bonds at temperatures between 350 °C and 800 °C.

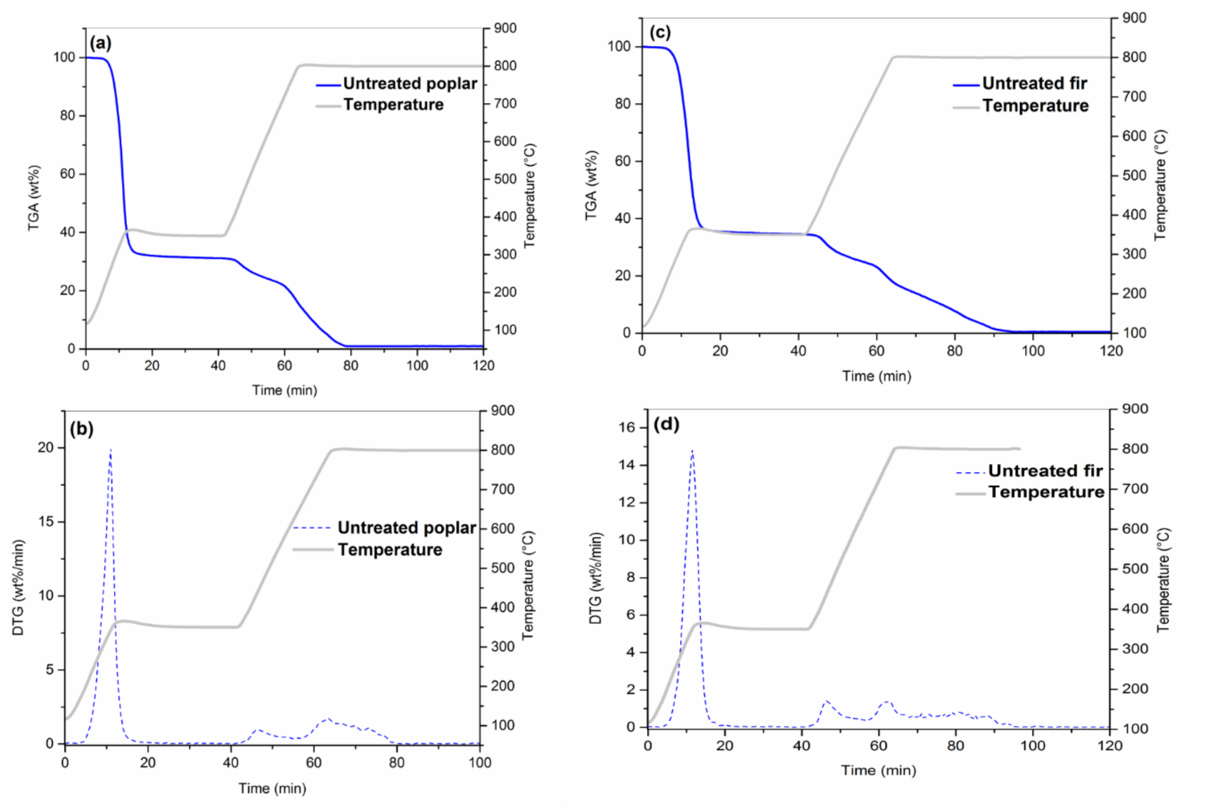

Figure 3. Raw sample of TGA (**a**) DTG, (**b**) curves of Poplar and TGA, (**c**) DTG, (**d**) curves of Fir.

One of the most notable results obtained from the raw data includes the similarity of the curves for different wood types, regardless of their classification as hard or soft woods. The most noticeable difference between the wood samples is the longer pyrolysis degradation for the Fir samples. In a CO_2 atmosphere, the torrefaction curve of these biomasses (105–350 °C, Figure 3) looks similar to those reported in the literature in an N_2 atmosphere [24,39]. This similarity agrees with what has been found during the torrefaction of other biomasses in a CO_2 atmosphere. In fact, it has been reported that CO_2 plays little role in physical properties during the torrefaction step [30,41]. However, during pyrolysis, the degradation of the remaining materials begins at approximately 450 °C, as expected, and continues until near completion at approximately 750 °C, unlike results reported under a nitrogen (N_2) atmosphere.

This continuing degradation can be attributed to the theoretical Boudouard equilibrium, which states that gaseous carbon dioxide (CO_2) will react with solid carbon to form carbon monoxide at temperatures greater than 700 °C, as seen in Equation (1) [42,43].

$$\mathrm{C(s)} + \mathrm{CO_2(g)} \leftrightharpoons \mathrm{2CO(g)} \tag{1}$$

Multiple studies have explored the feasibility of the Boudouard reaction and have concluded that heating rate and biomass source influence the temperature that marks the onset of the Boudouard equilibrium [44,45]. Cho et al. exposed spent coffee grounds to both nitrogen and carbon dioxide atmospheres with a heating rate of 10 °C/min from ambient temperature to 900 °C [31,46]. The study determined that the TGA curves between the two gases were similar until around 350 °C and that under carbon dioxide, the Boudouard equilibrium shifted right at approximately 850 °C, causing total degradation and a higher concentration of carbon monoxide gas produced under these conditions. Kim et al. observed oak tree sugars in both nitrogen and carbon dioxide atmospheres from ambient temperature to 900 °C with a heating rate of 35 °C/min [32]. The study found that mass decay from the Boudouard reaction begins at a temperature greater than 720 °C and reaches a maximum at 830 °C.

The aforementioned phenomena allowed all those studies to conclude that the Boudouard reaction has very slow reaction kinetics. Similar conclusions were reached by Cho et al. [31,46], who compared TGA curves of red seaweed in both nitrogen and carbon dioxide atmospheres. The study found heating rate to be a contributing factor in the onset of the Boudouard reaction with the right being favored at approximately 850 °C using a heating rate of 100 °C/min while a heating rate of 5 °C/min allowed for the onset to begin at 740 °C with complete degradation to carbon monoxide taking a total of 16 min, therefore validating the Boudouard reaction to have very slow reaction kinetics. These studies confirm the feasibility of the Boudouard equilibrium to favor carbon monoxide formation at approximately 750 °C and complete degradation in approximately 16 min after reaching 800 °C, as seen in the current study (Figure 3).

Compared to large-scale industrial processes, the environmental impact of experimental CO_2 utilization is probably going to be minimal. Even so, it's crucial to think about the possible effects and take precautions against them. The environmental impact of utilizing CO_2 for testing can be lessened, for instance, by using smaller volumes of CO_2, making sure that it is properly contained and disposed of, and using renewable energy for any related activities. Several concepts related to carbon capture, use, and storage (CCUS) have been put forth in earlier studies on the management of CO_2. The plan is to use pyrolyzed biochar to capture CO_2 directly from the air [47], use the catalytic chemical looping reaction to reduce industrial CO_2 emissions [48], and even use the CO_2 for the CO_2-expanded fluid extraction method in microalgae oil [49].

3.3. Catalytic Activity

From the three possible alkali earth metal and alkali metal catalysts, the presence of potassium had the greatest literature precedent in woody biomass torrefaction-pyrolysis. No known studies have explored how KCl affects the torrefaction-pyrolysis of woody biomass in a complete carbon dioxide atmosphere. Figure 4 shows the TGA/DTG curves of Poplar and Fir of different particle sizes impregnated with 0.05 M of KCl. It can be seen that the TGA degradation profile of these wood types is very similar, regardless of the particle size. There are three main degradation peaks on the DTG. There is a maximum of only 3% difference in weight loss between samples impregnated with KCl and raw wood. The presence of KCl causes less mass loss during torrefaction and more rapid degradation during pyrolysis for Poplar. During torrefaction, the weight loss of the sample impregnated with KCl was approximately 63.10% vs. 68.13% for the raw sample. The predicted error of the instrument is approximately 3%, therefore, the observed difference was deemed negligible. Upon increasing the concentration of KCl by two-fold to 0.1 M, the TGA and DTG curves (Figure 5) reveal a decrease of nearly 6.5% in mass loss during torrefaction with respect to the raw sample. This indicates that the presence of potassium in woody biomass causes a decrease in weight loss during torrefaction and an increase in the rate of degradation during pyrolysis.

In Figure 6, TGA and DTG curves of Poplar impregnated with different concentrations of NaCl are overlayed with the raw wood sample. The sample impregnated with 0.054 M of NaCl showed almost the same mass loss (69.47 wt.%) as the control (68.13 wt.%). When the concentration used was increased to 0.1 M, no difference was observed between the impregnated sample and the raw wood. In conclusion, NaCl did not have an observable impact on the thermal degradation of the woody biomass. Using the same procedures as the impregnations of NaCl and KCl, Poplar samples with a particle size of 500 µm were impregnated with a 0.054 M solution of $MgCl_2$. The DTG and TGA curves of these samples are presented in Figure 7. There was a very distinct difference between the raw wood and samples impregnated with $MgCl_2$ during both torrefaction and pyrolysis. Foremost, the presence of $MgCl_2$ increases weight loss during torrefaction by nearly 4.5%, from 68.13 wt.% for the raw wood to 72.60 wt.% for the impregnated sample. During pyrolysis, the initial degradation is similar between the raw wood and the impregnated sample. This degradation is presumed to be associated with the remaining crystalline cellulose regions in the biomass material. It is interesting to note that the complete degradation attributed to the Boudouard equilibrium is not present for samples impregnated with $MgCl_2$. Instead, the impregnated sample only attains complete degradation during combustion, as expected under a nitrogen atmosphere. The test was repeated with samples impregnated with 0.025 M and 0.012 M of $MgCl_2$, resulting in identical curves to those of the sample impregnated with 0.054 M of $MgCl_2$. This indicates that there is a saturation point for the effect of $MgCl_2$ in woody biomass. In order to determine the saturation point, Poplar samples were impregnated with 0.006 M and 0.003 M solutions. The sample impregnated with 0.003 M of $MgCl_2$ displays slightly more degradation before combustion. These concentrations were repeated with Fir with similar results in further discussion.

The lack of the Boudouard reaction for samples impregnated with $MgCl_2$ has not been extensively reported in the literature but was also observed by Aho et al. in the gasification of acid-washed pine doped with magnesium, potassium, and sodium [50]. The gasification was performed at 805 °C in an atmosphere containing 50% of N_2 and 50% of CO_2, in a TGA, with a heating rate of 50 °C/min. The rate of gasification of magnesium-doped samples lasted nearly five times longer than the rate of control, resulting in the need for further studies. However, some factors that could be contributing to the inhibition of the Boudouard equilibrium in the presence of $MgCl_2$ are the slow reaction kinetics of the Boudouard equilibrium in combination with the faster reaction kinetics of the magnesium ion in the presence of carbon dioxide in the redox reaction shown in Equation (2).

$$\mathrm{2Mg^{2+} + CO_2 \rightarrow 2MgO + C} \tag{2}$$

This reaction is very thermodynamically favorable and commonly reported in the literature, as magnesium is an element capable of oxidation in the presence of CO_2. Frost et al. determined that the combustion of magnesium in the air would begin to form magnesium oxide at 500 °C, and the reaction rate would increase at 560 °C. Under carbon dioxide, however, the enthalpy of the reaction is −810.1 kJ [51]. Barabulica et al. reported the reaction of magnesium in various mixtures of nitrogen and carbon dioxide and determined that no reaction occurred in atmospheres containing less than 10% carbon dioxide. As the carbon dioxide concentration increased, the reaction rate increased [52]. However, this is not the only reaction possible for an explanation of this phenomenon. While it is likely to be occurring, the low concentration of magnesium present in the sample should not be enough to outcompete all signs of the Boudouard reaction, and therefore, it is thought that the (2+) charge of the magnesium could play a role in this effect. Moreover, magnesium's affinity to bind to oxygen could cause the formation of a more oxygen rich material at the end of torrefaction, leaving less carbon to react in the Boudouard reaction and delay its occurrence to a time and temperature outside of the range of this study. In order to confirm any of these hypotheses, future studies need to be conducted to analyze the composition of materials after torrefaction using FTIR and py-GCMS during gasification.

The main novelty of the work presented herein lies in the lack of the Boudouard reaction for samples impregnated with $MgCl_2$. The evidence in the experiments performed points to an inhibition of the Boudouard reaction in the presence of Mg^{2+}, which was not observed with any of the other salts investigated. As discussed earlier, this finding is in line with reports on the inhibition of the Boudouard reaction during the gasification of pine in the presence of magnesium [50]. It has also been shown that the presence of Mg^{2+} during the pyrolysis of sawdust favored crosslinking and repolymerization reactions of pyrolysis intermediates, resulting in an increased biochar yield and the formation of the stable metal oxide MgO [53]. One possible mechanistic explanation for these observations is that the crosslinking, condensation, and repolymerization reactions catalyzed by magnesium happen at a faster rate than the Boudouard reaction, offsetting its effect and resulting, globally, in a higher rate of biochar/solid carbon formation than the rate of solid carbon conversion to CO through the Boudoard reaction.

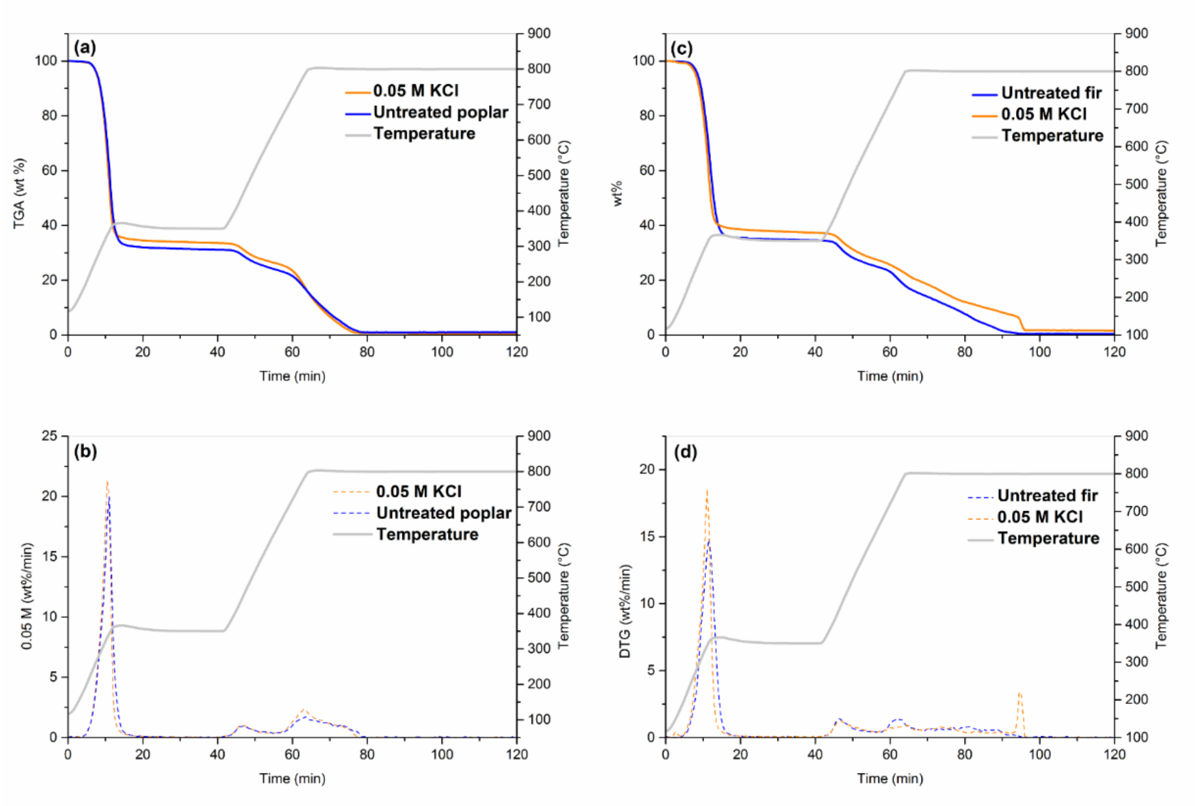

Figure 4. KCl 0.05 M impregnated of TGA (**a**) DTG, (**b**) curves of Poplar and TGA, (**c**) DTG, (**d**) curves of Fir.

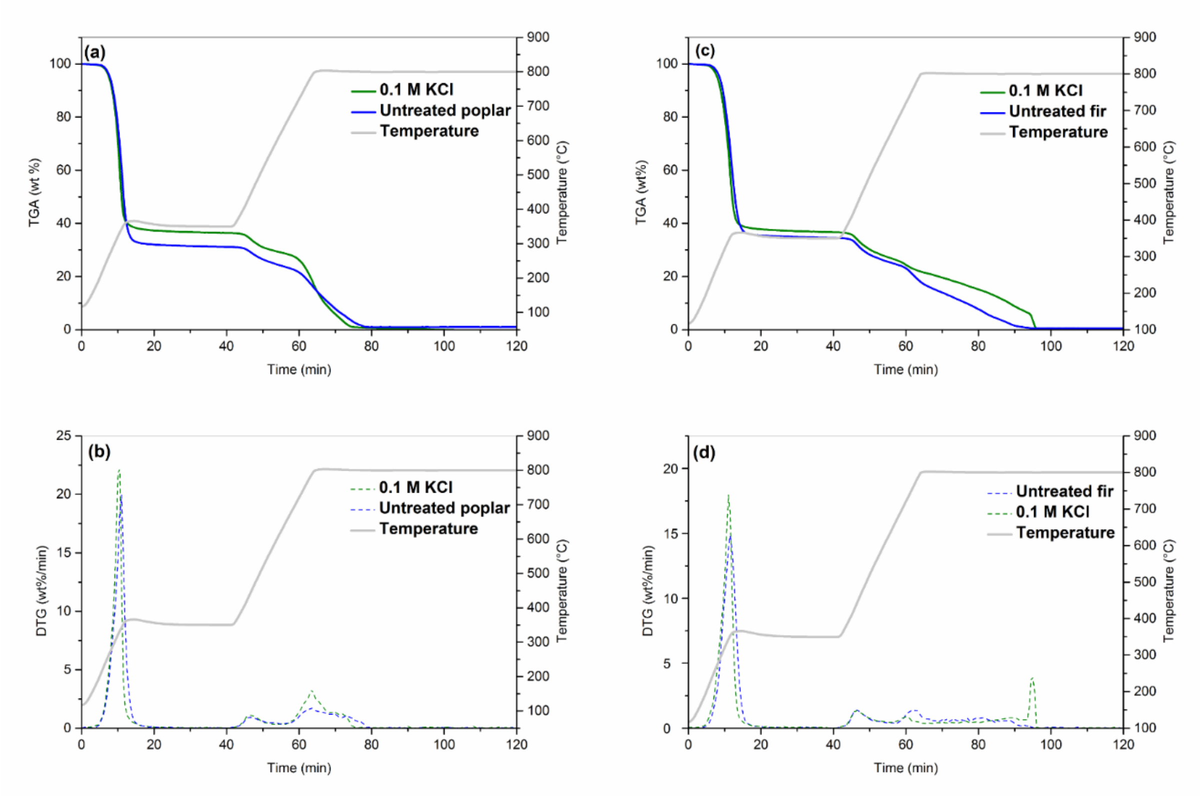

Figure 5. KCl 0.1 M impregnated of TGA (**a**) DTG, (**b**) curves of Poplar and TGA, (**c**) DTG, (**d**) curves of Fir.

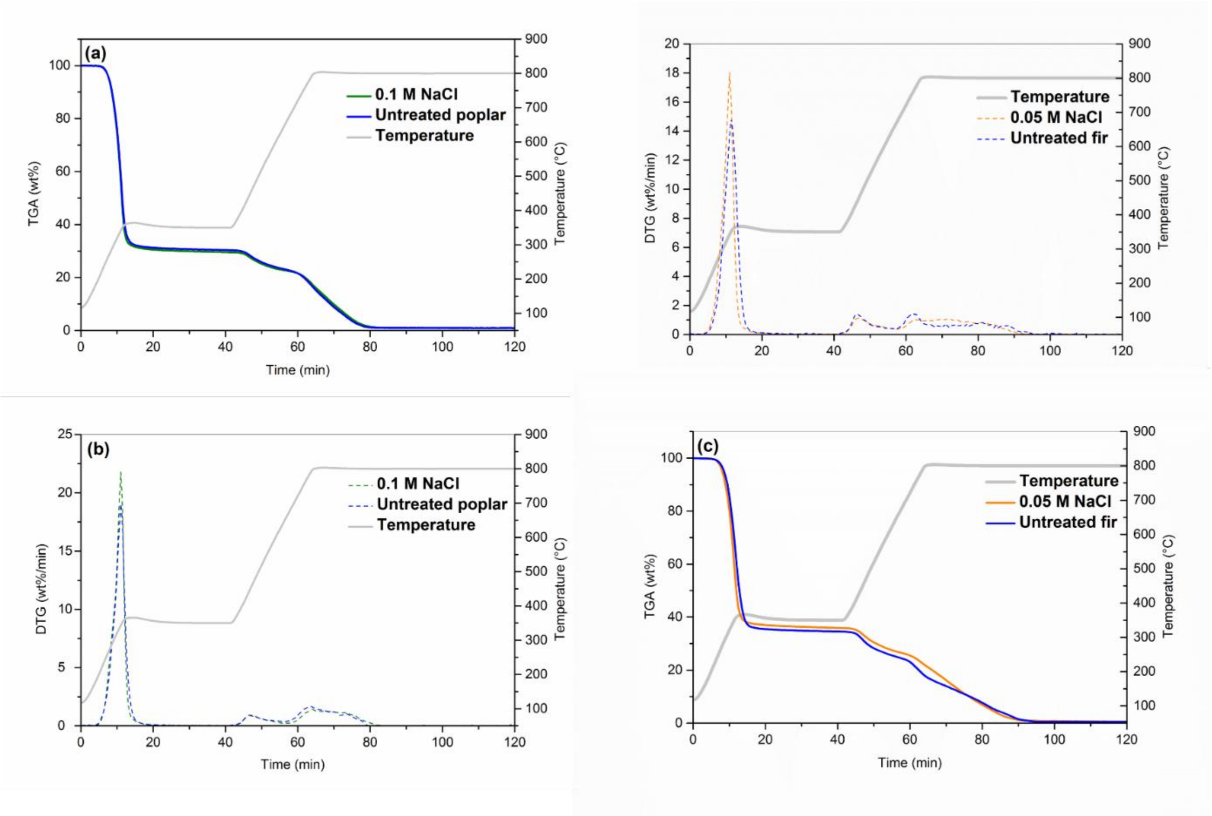

Figure 6. NaCl 0.1 M impregnated of TGA (**a**) DTG, (**b**) curves of Poplar and NaCl 0.05 M impregnated of TGA, (**c**) DTG, (**d**) curves of Fir.

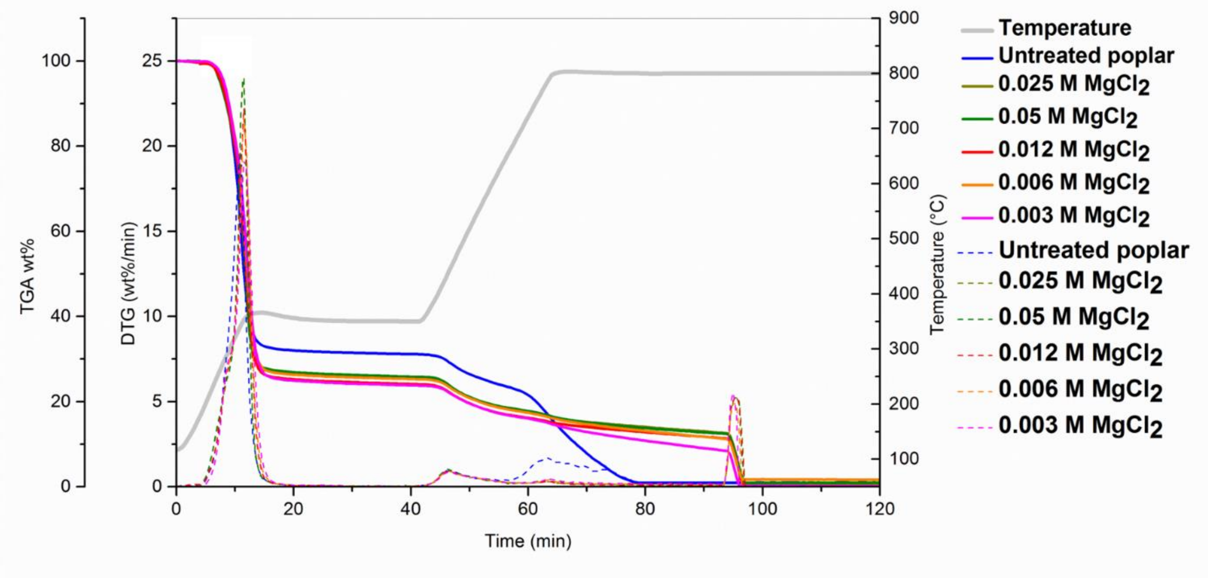

Figure 7. TGA and DTG curves of Poplar impregnated with different concentrations of $MgCl_2$.

3.4. Interaction Effect

The interaction effect from the catalysts can be defined as either synergistic or antagonistic. Synergistic effects are defined as a greater and/or faster degradation of the material treated with external material, in this study, such as the catalyst, than the untreated sample (raw) in a certain range, while, antagonistic effects are defined as less and/or slower degradation of the material treated with the catalyst than that of the untreated sample [54,55]. If degradation is the same for both treated and untreated samples, it can be said that there is no interaction effect between the catalyst and the sample [54]. Aniza et al. [54] analyzed the interaction effect of three extracted components from microalgae (lipid, protein, and carbohydrate) during thermochemical conversion using TGA. According to the study, the synergistic impact happens when glucose signals as a dominant molecule in the carbohydrate model, accounting for roughly 50% of the total mass loss. These findings motivate the current study's use of catalyst impregnation to examine the interaction effect within woody biomass. Figure 8A shows the TGA and DTG curves of Poplar at a particle size of 500 µm after impregnation with different concentrations of KCl. It can be noted that the curve for the sample impregnated with 0.1 M KCl is the most different from the control, with the curve for the sample impregnated with 0.025M KCl being the most similar.

To determine how impregnation with 0.1 M KCl affects both torrefaction and pyrolysis separately, the graph can be analyzed in two parts, with enlarged graphs of torrefaction (Figure 8B) and pyrolysis (Figure 8C). In Figure 8B, the DTG curve for the sample impregnated with 0.1 M of KCl is shifted left of the control, with a sharper peak. This shift indicates degradation is happening more rapidly and at a lower temperature, leading to the conclusion that KCl has a synergistic catalytic effect on Poplar for samples impregnated with 0.1 M and 0.05 M of KCl. The effect increases with increasing concentrations of KCl. It can be noted, however, that there appears to be less mass loss in samples containing KCl than in the control during torrefaction. This was similarly reported by a multitude of sources in both complete nitrogen and oxidative atmospheres and confirms that the impregnation of potassium contributes to weakening linkages and hydrogen bonding between cellulose and hemicellulose components [22,24]. In a purely speculative way, it can be proposed that the chemical pathway for K^+ to disrupt hydrogen bonds in cellulose and hemicelluloses occurs by replacing H^+, therefore opening the microfibril structure and making it more susceptible to thermal degradation.

The pyrolysis step can be observed in Figure 8C, where KCl appears to have a synergistic effect on the degradation of Poplar at approximately 800 °C. While this temperature is attributed to gasification in a carbon dioxide atmosphere, the implications of potassium at this temperature in lignocellulosic biomass are not commonly reported. However, Menendez et al. observed the microwave-assisted pyrolysis of coffee hulls with carbon dioxide and determined that potassium-rich samples catalyze self-gasification reactions like the Boudouard equilibrium [56]. It could be hypothesized that the degradation of potassium-rich samples during torrefaction leads to a more carbon-rich char participating in Boudouard gasification a enhancing the rate of degradation.

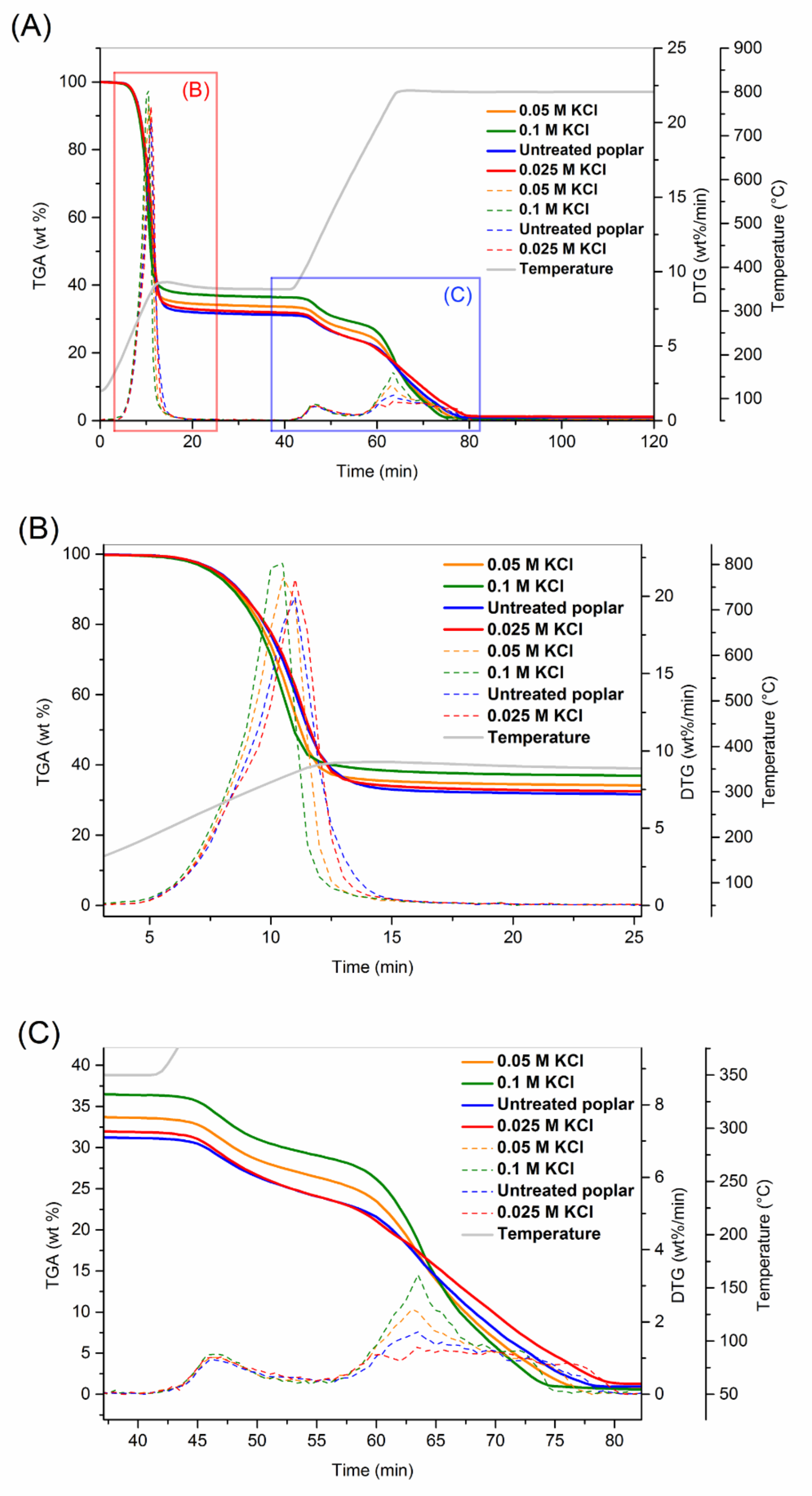

Figure 8. (**A**) TGA and DTG curves of Poplar impregnated with 0.1 M, 0.05 M, and 0.025 M solutions of KCl, (**B**) Enlarged section (torrefaction) Poplar, and (**C**) Enlarged section (pyrolysis) Poplar.

These results can be contrasted with Figure 9A, which shows the TGA and DTG curves of Fir samples impregnated with KCl at different concentrations. While Figure 9B shows a clear synergistic effect during torrefaction similar to the one observed with Poplar, in Figure 9A, an antagonistic effect can be seen during the pyrolysis (~800 °C) of Fir samples impregnated with KCl. This indicates a fundamental difference between Fir and Poplar. Dupont et al. studied the gasification kinetics of different hard and soft woods. It was found that higher concentrations of silica had an inhibitory effect on gasification reactions despite the catalytic presence of potassium because of the formation of potassium silicates. The concentration of inorganic salts in both Poplar and generalized "soft woods" were measured and it was found that soft woods have approximately 3619 mg Si/kg of dry biomass while Poplar has 763 mg Si/kg of dry biomass (nearly a 5-fold difference in silica content) [57]. It could be hypothesized that the silica content in Fir could have an inhibitory effect on the gasification reactions during pyrolysis.

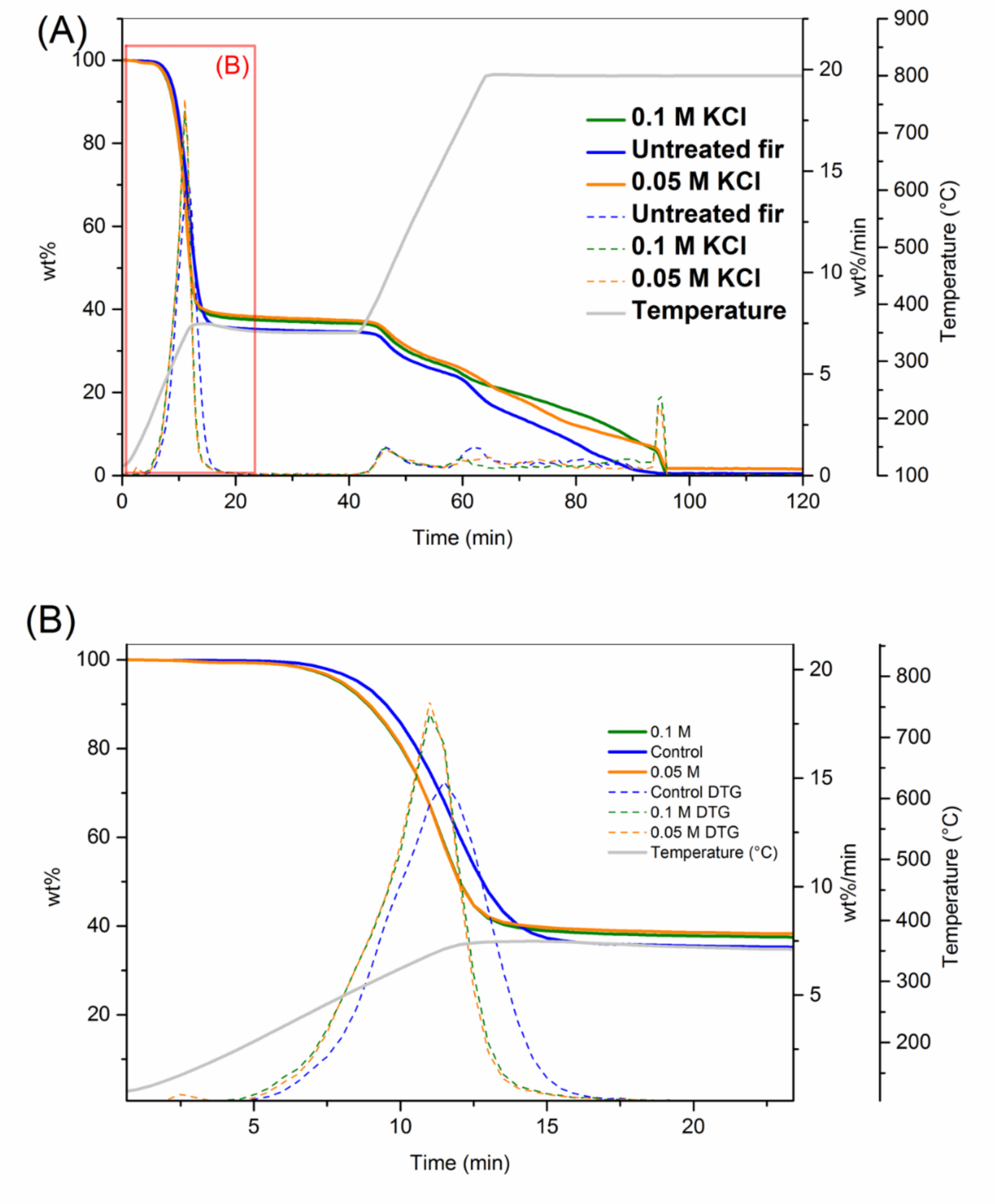

Figure 9. (**A**) TGA and DTG curves of Fir impregnated with 0.1 M, 0.05 M of KCl, and (**B**) Enlarged section (torrefaction) Fir.

In Figure 10A, the torrefaction-pyrolysis curve of NaCl impregnated Poplar samples is shown. It was stated that the difference in results is negligible, indicating that NaCl does not have strong effects on the torrefaction-pyrolysis of Poplar in a carbon dioxide environment. When looking at only the torrefaction curve of NaCl impregnated samples vs the control in Figure 10B, it can be seen that there are very slight synergistic effects in the DTG curve but that these are negligible. The same can be noticed in the Figure 10C with the pyrolysis of these samples—there is a slight synergistic effect around 800 °C, but by a negligible amount. The TGA-DTG curve of NaCl impregnated Fir samples can be seen in Figure 11A. In Figure 11B, the torrefaction step presents a slight synergistic effect, while there is a slight antagonistic effect from the NaCl during the Pyrolysis step in Figure 11A. This indicates the effects of NaCl in the pyrolysis of impregnated Fir to be the opposite of impregnated Poplar, although both are so slight that they are negligible.

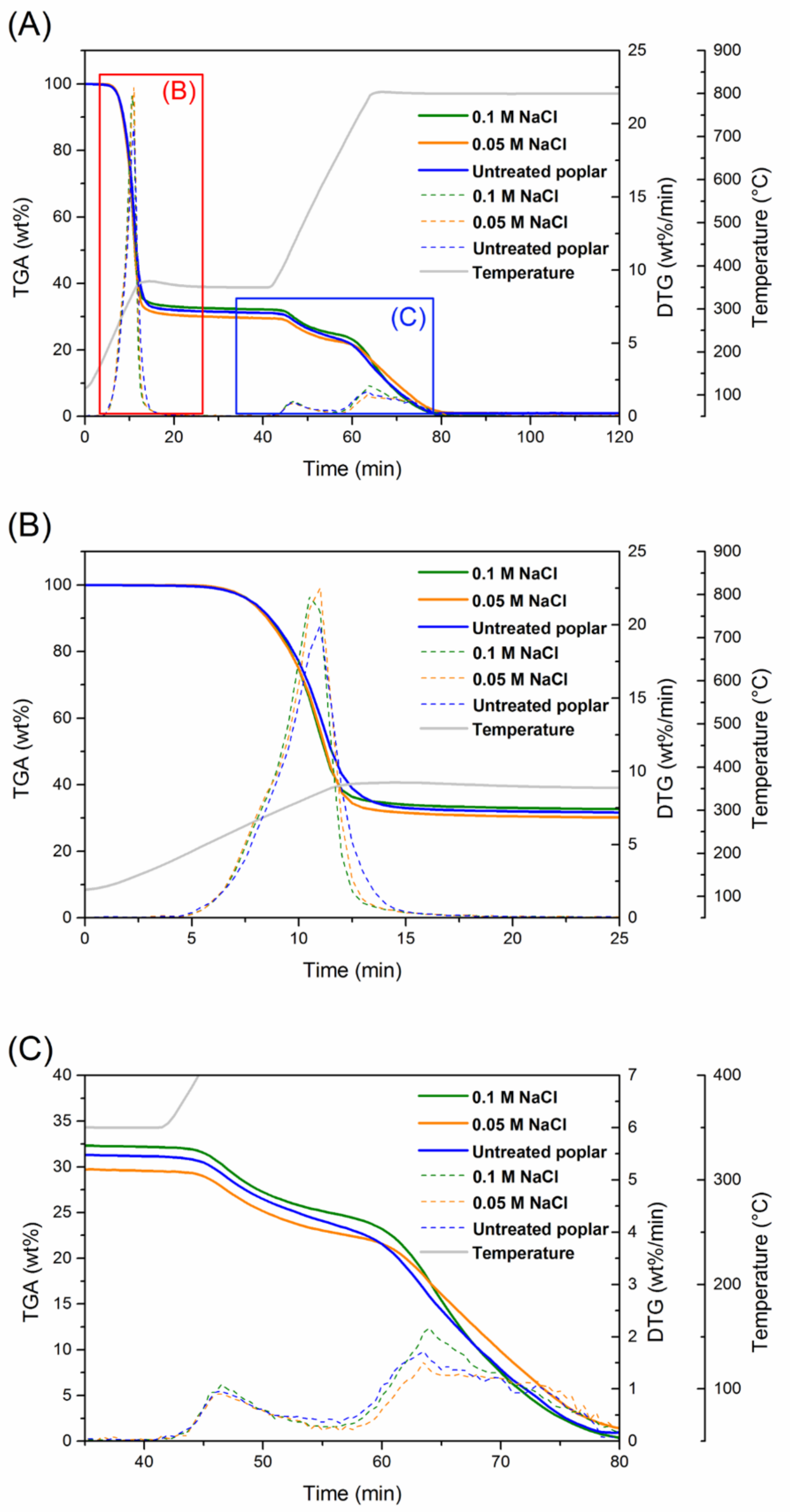

Figure 10. (**A**) Torrefaction-Pyrolysis TGA and DTG curves of Poplar impregnated NaCl with 0.1 M and 0.05 M, (**B**) Enlarged section (torrefaction) Poplar, and (**C**) Enlarged section (pyrolysis) Poplar.

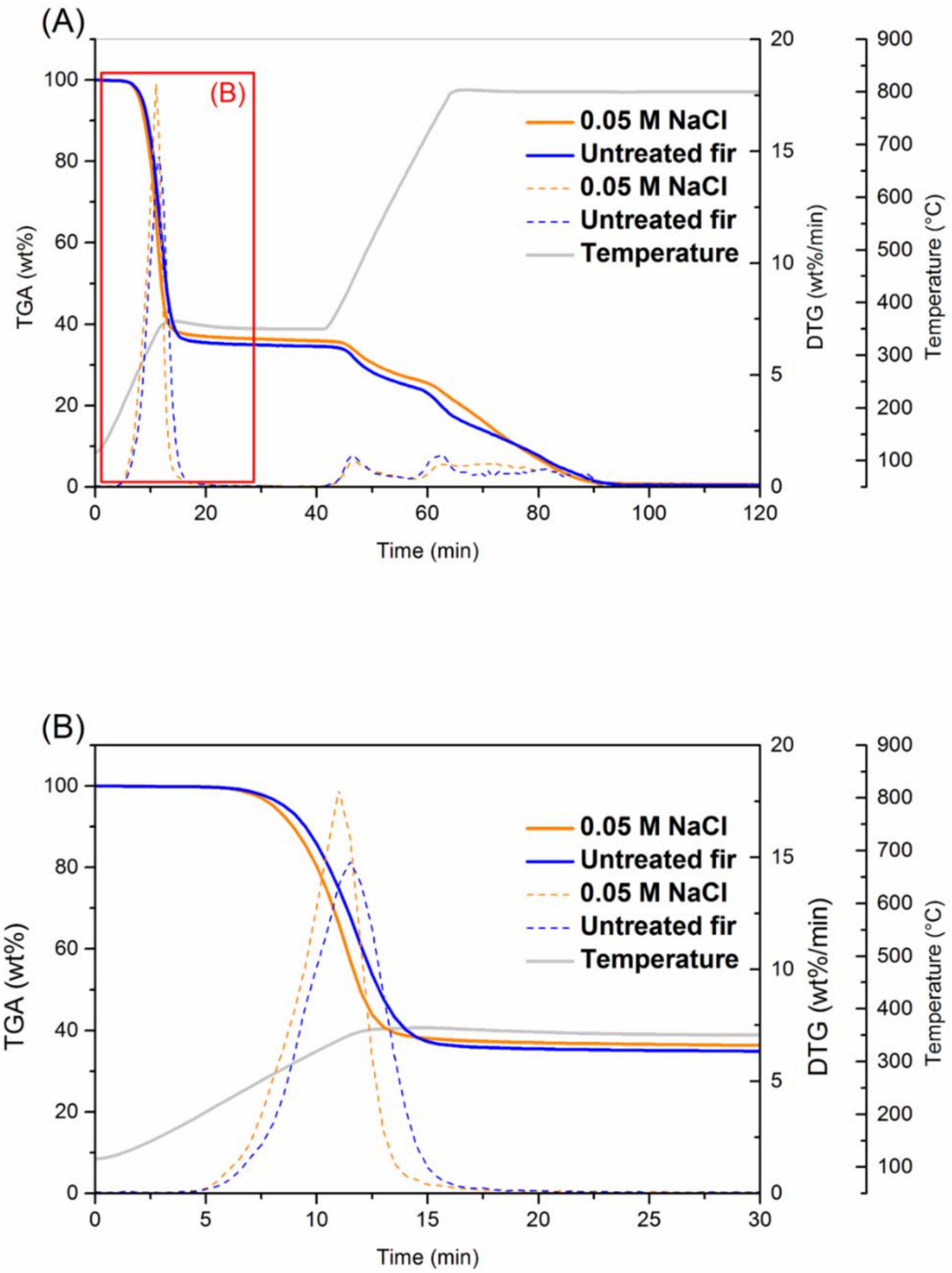

Figure 11. (**A**) Torrefaction-pyrolysis curve of Fir treated with NaCl and (**B**) Torrefaction curve of Fir treated with NaCl.

Figure 12 shows the torrefaction curve of $MgCl_2$-impregnated Poplar samples as an expanded graph of the entire torrefaction-pyrolysis seen in Figure 7. While $MgCl_2$ increases weight loss during the torrefaction step, there is a slight antagonistic effect of $MgCl_2$ on the rate of torrefaction see in Figure 12 with the DTG curve of the impregnated samples showing a cellulose peak shift right (indicating higher temperatures for degradation) and the appearance of a hemicellulose shoulder in the impregnated samples that is not shown in the impregnated samples. This indicates that $MgCl_2$ affects the degradation of hemicelluloses—similar to those results by Kawamoto et al. [58]. These results can be contrasted with those with Fir in Figure 13. Figure 13A shows the entirety of the $MgCl_2$-impregnated Fir torrefaction-pyrolysis graph which appears similar to that of $MgCl_2$-impregnated Poplar. However, in Figure 13B, the enlarged torrefaction TGA and DTG curves show $MgCl_2$ to have a synergistic effect with the lack of a hemicellulose shoulder.

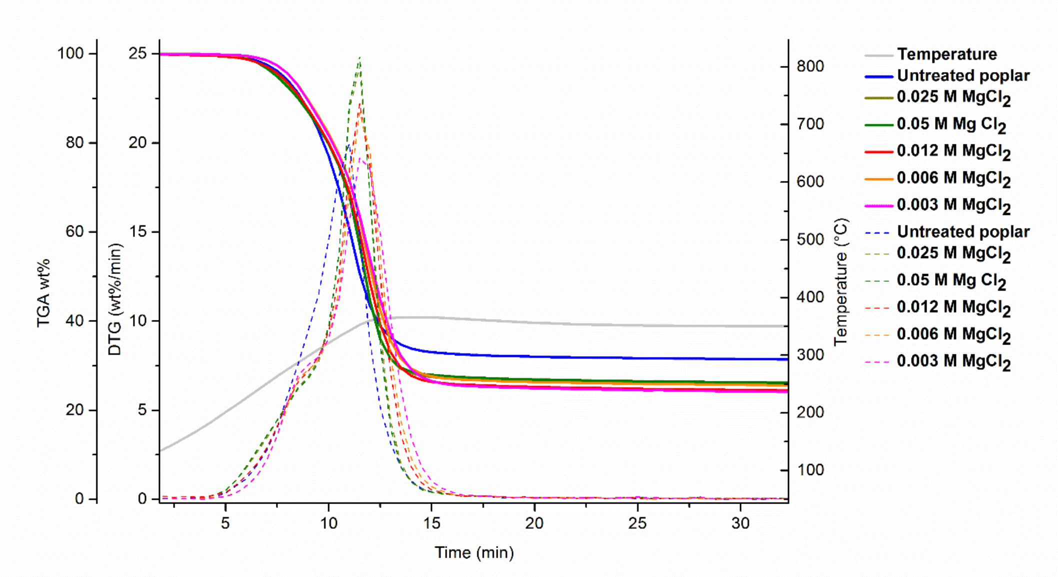

Figure 12. Torrefaction curve of Poplar treated with $MgCl_2$ solutions.

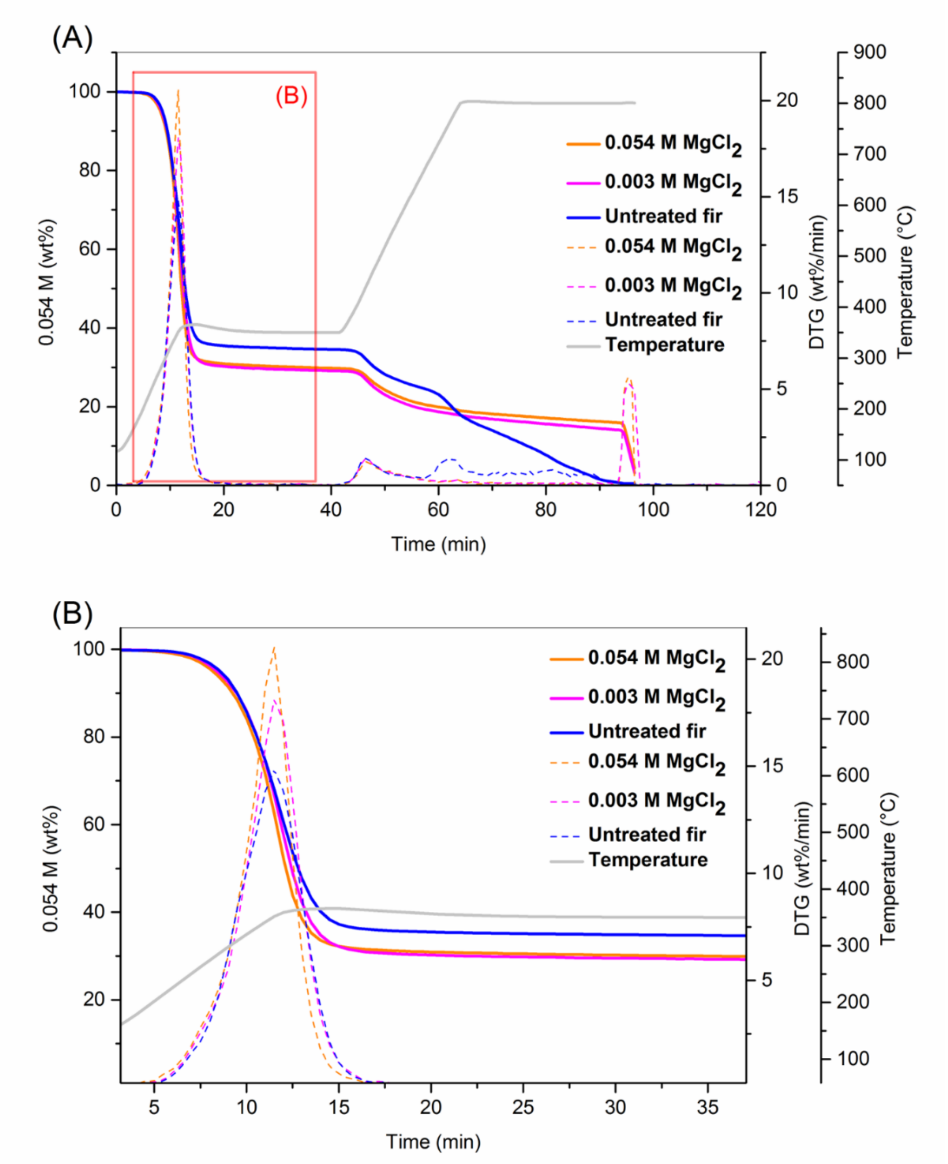

Figure 13. (**A**) TGA-DTG curves of torrefaction-pyrolysis of Fir treated with $MgCl_2$ and (**B**) TGA DTG curves of torrefaction of Fir treated with $MgCl_2$.

A comparison of all catalytic impregnations of Poplar wood can be found in Figure 14. During torrrefaction, a synergistic effect is observed from impregnation with KCl with an antagonistic effect from impregnation with $MgCl_2$—where the hemicellulose shoulder is much more prominent than in the control sample seen in Figure 15A. This appearance of a broad shoulder could indicate the prolonged degradation of hemicellulose with a delayed degradation of cellulose when magnesium is present. During the pyrolysis segment, all impregnations displayed similar degradation rates as the control, but gasification was accelerated when exposed to KCl and inhibited when exposed to $MgCl_2$ as seen in Figure 15B. Catalytic activity when impregnated in Fir was drastically different from that of Poplar as seen in Figure 16. During the torrefaction step shown in Figure 17A, KCl has a greater synergistic effect than $MgCl_2$—while $MgCl_2$ results in greater mass loss. During the pyrolysis step in Figure 17B, the rate of degradation is similar for all samples. Upon gasification, $MgCl_2$ samples show an absence of gasification, while KCl shows an antagonistic effect in comparison to NaCl and the raw samples.

In terms of ionic reaction, when comparing the effects of KCl, NaCl, and $MgCl_2$ during the torrefaction of wood, the different behavior observed can be attributed primarily to the cations K^+, Cl^+, and Mg^{2+} since the anion Cl^- is the same in all cases. For the Boudouard reaction inhibition, as discussed previously, it is believed that the charge (+2) of magnesium is critical in catalyzing condensation, crosslinking, and repolymerization reactions. Likewise, K^+ is believed to disrupt H-bonding while Na^+ doesn't have that effect, which could be related to specific cation properties such as radius. In order to fully elucidate these factors, a comprehensive screening of a series of compounds would be necessary.

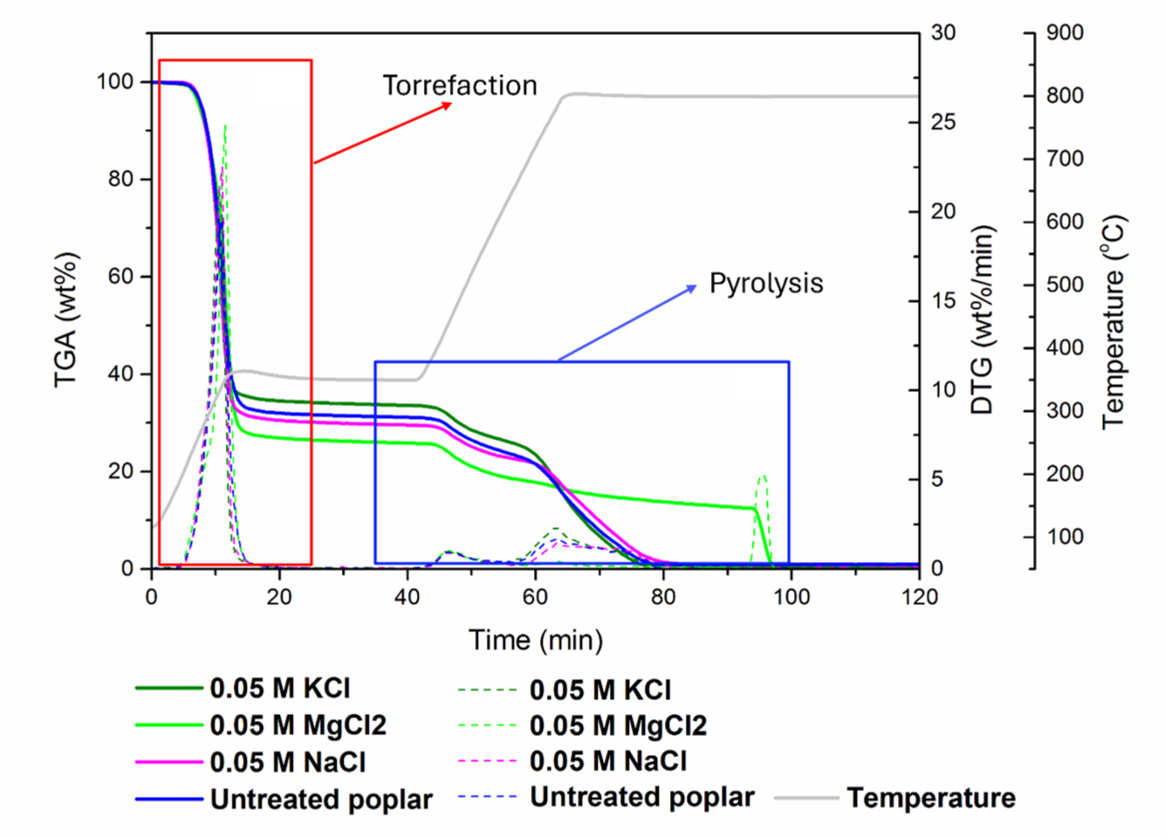

Figure 14. Torrefaction-pyrolysis TGA and DTG curves of Poplar treated with $MgCl_2$, NaCl, KCl.

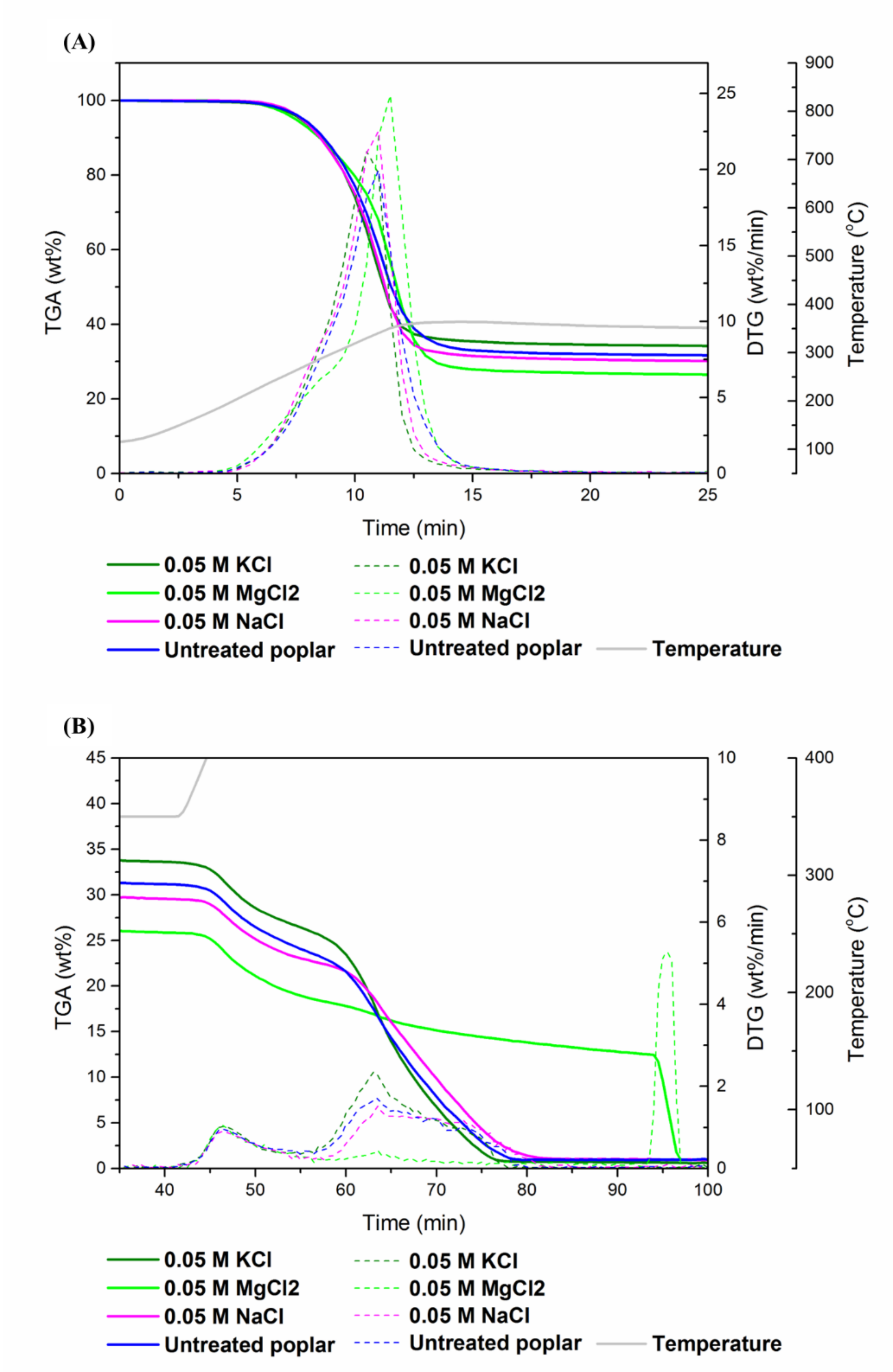

Figure 15. (**A**) TGA-DTG torrefaction curve of Poplar treated with $MgCl_2$, NaCl, KCl and (**B**) TGA-DTG pyrolysis curve of Poplar treated with $MgCl_2$, NaCl, KCl.

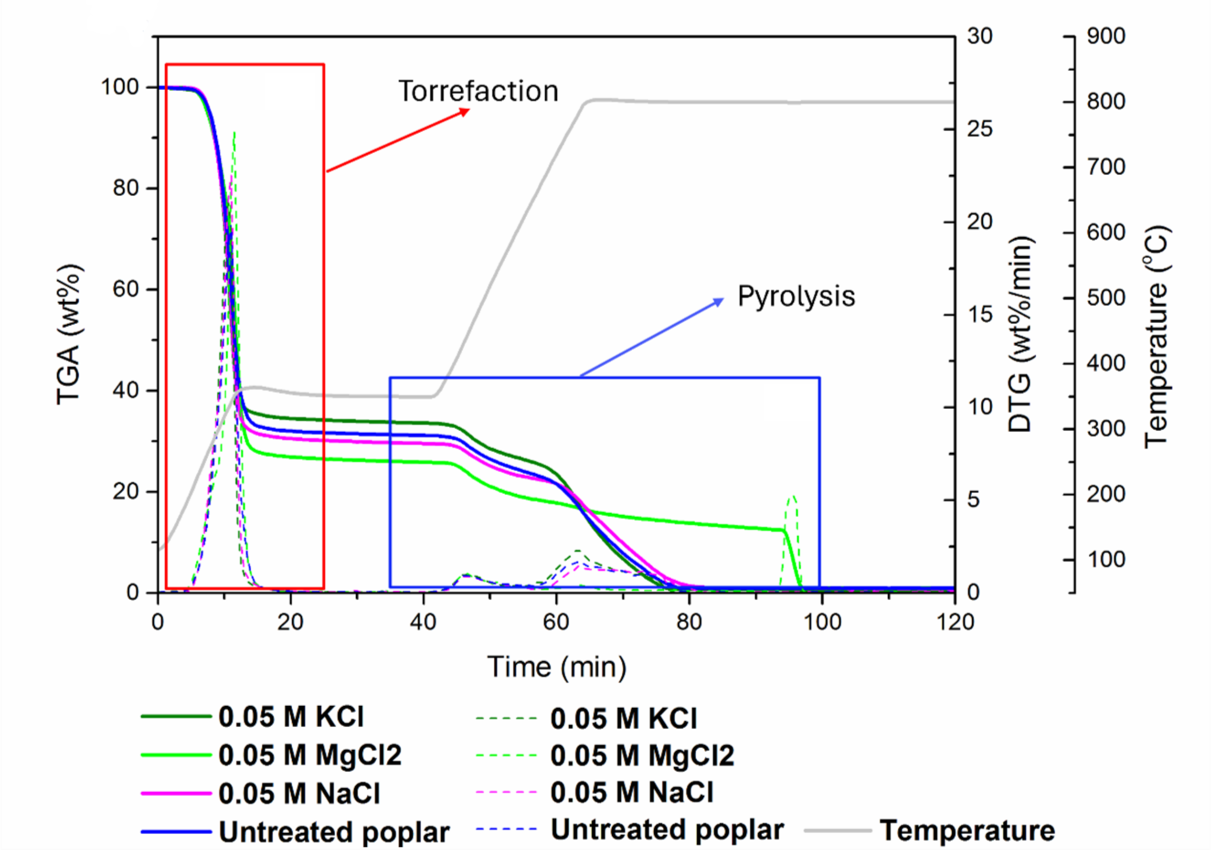

Figure 16. Torrefaction-pyrolysis TGA and DTG curves of Fir treated with $MgCl_2$, NaCl, KCl.

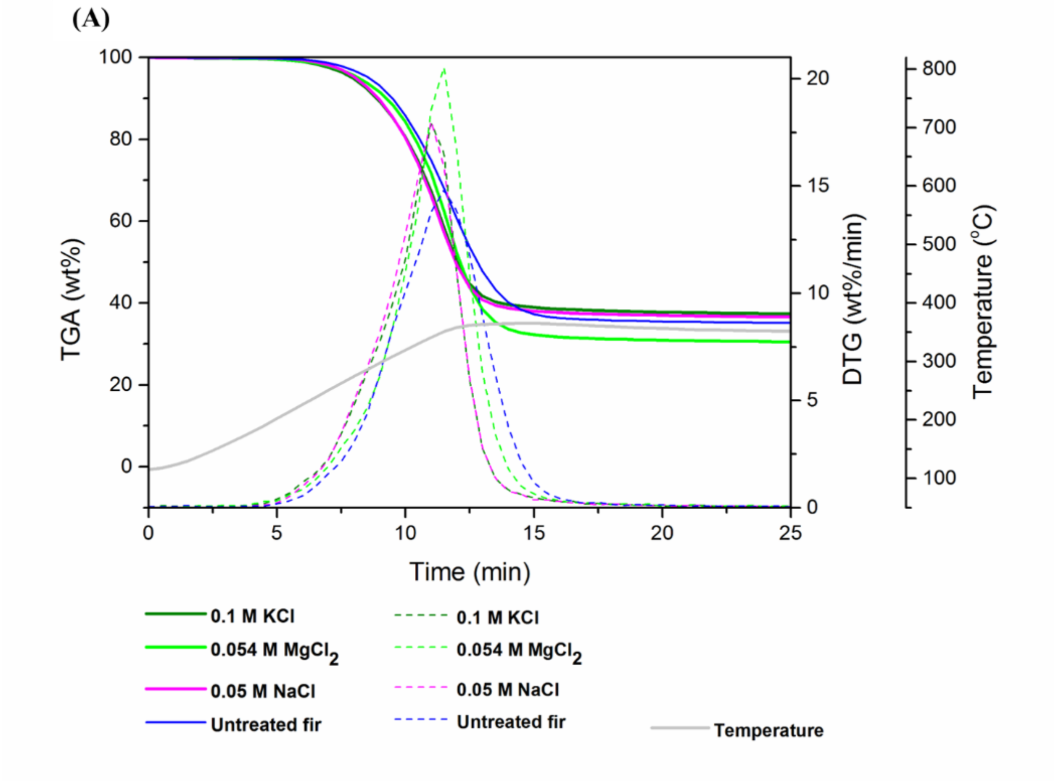

Figure 17. *Cont.*

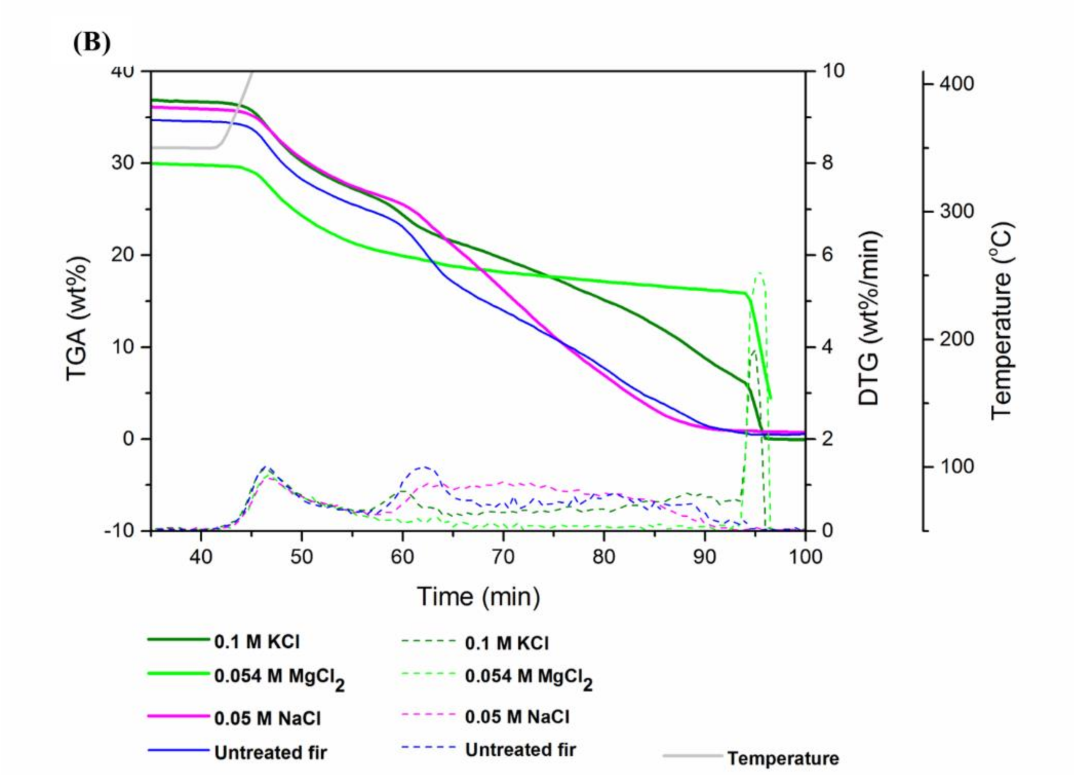

Figure 17. (**A**) TGA-DTG torrefaction curve of Fir treated with $MgCl_2$, NaCl, KCl and (**B**) TGA-DTG pyrolysis curve of Fir treated with $MgCl_2$, NaCl, KCl.

4. Conclusions

Poplar and Fir wood species have different chemical compositions, which cause a difference in catalytic efficiency when exposed to different alkali and alkaline earth metals—namely, K, Na, and Mg. Both Poplar and Fir species show self-gasification in a carbon dioxide environment at temperatures greater than 700 °C. When employing catalytic thermal conversion to produce biofuel, the aK-catalyst outperforms the other catalyst materials (K, Na, and Mg) in a CO_2 atmosphere. When the K-catalyst is impregnated in Fir, the C-O-C compound decreases. This is in line with the fact that Fir's hemicellulose content (22.43 wt.%) is double that of Poplar (12.18 wt.%), which results in a less thermally stable molecule. This suggests that K may be able to have less interaction with CO_2 and better thermal resistance. K-impregnated Poplar samples showed faster self-gasification, possibly indicating a more carbon-rich state of biochar after torrefaction. Na-impregnated Poplar and Fir samples exhibited no self-gasification at magnesium loadings as little as 0.003 M impregnations. An explanation for this is currently unclear, and the observation is limited. The Boudouard equilibrium was detected in the thermal conversion at 780 °C. Furthermore, during torrefaction and pyrolysis, the synergistic impact is more noticeable when the K-catalyst is employed than when Na and Mg are used. This suggests that the K-catalyst's performance in this study is thermally stable. Further studies are suggested to be conducted at higher concentrations and using py-GCMS for an understanding of the underlying mechanisms in CO_2.

Author Contributions: E.W.S. experimental investigation, writing—original draft preparation; R.A. conceptualization, methodology, writing—original draft preparation; A.P. conceptualization, supervision, validation; R.L.Q. conceptualization, supervision, writing—reviewing; B.C. experimental; M.P., supervision, validation; W.-H.C. supervision, validation. All authors have read and agreed to the published version of the manuscript.

Funding: This research was funded by ANR-11-LABEX-0002-01 (Lab of Excellence ARBRE) in France, the National Science Foundation (NSF) under the grant NSF-IRES 1952402 (I-CEMITURE (International-CEMITURE)) awarded by the NSF Office of International Science & Engineering (OISE), Georgia Southern University USA.

Institutional Review Board Statement: Not applicable.

Informed Consent Statement: Not applicable.

Data Availability Statement: Not applicable.

Conflicts of Interest: The authors declare no conflict of interest.

References

1. Nullis, C. WMO Greenhouse Gas Bulletin. More Bad News for the Planet: Greenhouse Gas Levels Hit New Highs. Switzerland: World Meteorological Organization 2022. Available online: https://wmo.int/news/media-centre/more-bad-news-planet-greenhouse-gas-levels-hit-new-highs (accessed on 30 April 2025).
2. Aniza, R.; Chen, W.-H.; Pétrissans, A.; et al. A review of biowaste remediation and valorization for environmental sustainability: Artificial intelligence approach. *Environ. Pollut.* **2023**, *324*, 121363. https://doi.org/10.1016/j.envpol.2023.121363.
3. Vuppaladadiyam, A.K.; Vuppaladadiyam, S.S.V.; Sahoo, A.; et al. Bio-oil and biochar from the pyrolytic conversion of biomass: A current and future perspective on the trade-off between economic, environmental, and technical indicators. *Sci. Total Environ.* **2023**, *857*, 159155. https://doi.org/10.1016/j.scitotenv.2022.159155.
4. Congyu, Z.; Jin, F.; Yong, Z.; et al. Life Cycle Assessment of Microalgal Carbon Fixation and Torrefaction for Carbon Neutralization: A State-of-the-Art Review. *Green Energy Fuel Res.* **2024**, *1*, 23–38. https://doi.org/10.53941/gefr.2024.100004.
5. Tubbesing, C.L.; Lara, J.D.; Battles, J.J.; et al. Characterization of the woody biomass feedstock potential resulting from California’s drought. *Sci. Rep.* **2020**, *10*, 1096. https://doi.org/10.1038/s41598-020-57904-z.
6. Lin, S.L.; Aniza, R.; Lee, Y.Y.; et al. Reduction of traditional pollutants and polychlorinated dibenzo-p-dioxins and dibenzofurans emitted from a diesel engine generator equipped with a catalytic ceramic fiber filter system. *Clean Technol. Environ. Policy* **2018**, *20*, 1297–1309. https://doi.org/10.1007/s10098-018-1559-6.
7. Lee, Y.Y.; Lin, S.L.; Aniza, R.; et al. Reduction of atmospheric PM2.5 level by restricting the idling operation of buses in a busy station. *Aerosol Air Qual. Res.* **2017**, *17*, 2424–2437. https://doi.org/10.4209/aaqr.2017.09.0301.
8. Aniza, R.; Chen, W.-H.; Herrera, C.J.A.; et al. Bioenergy and bioexergy analyses with artificial intelligence application on combustion of recycled hardwood and softwood wastes. *Renew. Energy* **2024**, *237*, 121885. https://doi.org/10.1016/j.renene.2024.121885.
9. Pétrissans, A.; Lin, Y.-Y.; Nguyen, T.N.; et al. Influence of the heating rate on the thermodegradation during the mild pyrolysis of the wood. *Wood Mater. Sci. Eng.* **2023**, *18*, 412–421. https://doi.org/10.1080/17480272.2022.2039289.
10. Aniza, R.; Petrissans, A.; Petrissans, M. Multifunctional Nanotechnology Application for Wood Properties Enhancement: Adhesive and Coating. In *Nanomaterials Additives in Bioadhesives for Wood Composites*; Antov, P., Lubis, M.A.R., Lee, S.H., Taghiyari, H.R., Eds.; Springer Nature: Singapore, 2025; pp. 135–149.
11. Aniza, R.; Petrissans, A.; Petrissans, M. Life-Cycle Assessment of Nanoparticle in Wood Adhesive and Coating: The State-of-The Art. In *Nanomaterials Additives in Bioadhesives for Wood Composites*; Antov, P., Lubis, M.A.R., Lee, S.H., Taghiyari, H.R., Eds.; Springer Nature: Singapore, 2025; pp. 231–248.
12. Andrade Breves, R.; Ajiola, D.; de Vasconcelos Vieira Lopes, R.; et al. Bio-Based Polyurethane Composites from Macauba Kernel Oil: Part 1, Matrix Synthesis from Glycerol-Based Polyol. *J. Compos. Sci.* **2024**, *8*, 363.
13. Aniza, R.; Chen, W.-H.; Kwon, E.E.; et al. Lignocellulosic biofuel properties and reactivity analyzed by thermogravimetric analysis (TGA) toward zero carbon scheme: A critical review. *Energy Convers. Manag. X* **2024**, *22*, 100538. https://doi.org/10.1016/j.ecmx.2024.100538.
14. Chen, W.-H.; Escalante, J.; Xuan, L.L.; et al. Catalytic co-gasification optimization of biomass and polyethylene wastes in oxygen-rich environments. *Fuel* **2025**, *381*, 133214. https://doi.org/10.1016/j.fuel.2024.133214.
15. McKendry, P. Energy production from biomass (part 1): Overview of biomass. *Bioresour. Technol.* **2002**, *83*, 37–46. https://doi.org/10.1016/S0960-8524(01)00118-3.
16. Chen, W.-H.; Lin, B.-J.; Lin, Y.-Y.; et al. Progress in biomass torrefaction: Principles, applications and challenges. *Prog. Energy Combust. Sci.* **2021**, *82*, 100887. https://doi.org/10.1016/j.pecs.2020.100887.
17. Acharya, B.; Dutta, A.; Minaret, J. Review on comparative study of dry and wet torrefaction. *Sustain. Energy Technol. Assess.* **2015**, *12*, 26–37. https://doi.org/10.1016/j.seta.2015.08.003.
18. Wang, L.; Riva, L.; Skreiberg, Ø.; et al. Effect of Torrefaction on Properties of Pellets Produced from Woody Biomass. *Energy Fuels* **2020**, *34*, 15343–15354. https://doi.org/10.1021/acs.energyfuels.0c02671.
19. Cahyanti, M.N.; Doddapaneni, T.R.K.C.; Kikas, T. Biomass torrefaction: An overview on process parameters, economic and environmental aspects and recent advancements. *Bioresour. Technol.* **2020**, *301*, 122737. https://doi.org/10.1016/j.biortech.2020.122737.
20. Amit Kumar, S. Solar Thermal Technologies for Biofuel Production: Recent Advances and Future Prospectus. *Green Energy Fuel Res.* **2025**, *2*, 13–25. https://doi.org/10.53941/gefr.2025.100002
21. Chen, W.-H. Progress in Green Energy and Fuel for Sustainability. *Green Energy Fuel Res.* **2024**, *1*, 13–22. https://doi.org/10.53941/gefr.2024.100003.

22. Richa, L.; Colin, B.; Pétrissans, A.; et al. Potassium carbonate impregnation and torrefaction of wood block for thermal properties improvement: Prediction of torrefaction performance using artificial neural network. *Appl. Energy* **2023**, *351*, 121894. https://doi.org/10.1016/j.apenergy.2023.121894.
23. Nishimura, M.; Iwasaki, S.; Horio, M. The role of potassium carbonate on cellulose pyrolysis. *J. Taiwan Inst. Chem. Eng.* **2009**, *40*, 630–637.
24. Richa, L.; Colin, B.; Pétrissans, A.; et al. Catalytic and char-promoting effects of potassium on lignocellulosic biomass torrefaction and pyrolysis. *Environ. Technol. Innov.* **2023**, *31*, 103193. https://doi.org/10.1016/j.eti.2023.103193.
25. Guo, F.; Liu, Y.; Wang, Y.; et al. Pyrolysis kinetics and behavior of potassium-impregnated pine wood in TGA and a fixed-bed reactor. *Energy Convers. Manag.* **2016**, *130*, 184–191. https://doi.org/10.1016/j.enconman.2016.10.055.
26. Zhao, N.; Li, B.-X. The effect of sodium chloride on the pyrolysis of rice husk. *Appl. Energy* **2016**, *178*, 346–352. https://doi.org/10.1016/j.apenergy.2016.06.082.
27. Zhu, C.; Huang, K.; Xue, M.; et al. Effect of $MgCl_2$ Loading on the Yield and Performance of Cabbage-Based Biochar. *Bioengineering* **2023**, *10*, 836. https://doi.org/10.3390/bioengineering10070836.
28. Pradana, Y.S.; Daniyanto; Hartono, M.; Prasakti, L.; et al. Effect of calcium and magnesium catalyst on pyrolysis kinetic of Indonesian sugarcane bagasse for biofuel production. *Energy Procedia* **2019**, *158*, 431–439. https://doi.org/10.1016/j.egypro.2019.01.128.
29. Müller, T.E.; Leitner, W. CO_2 Chemistry. *Beilstein J. Org. Chem.* **2015**, *11*, 675–677. https://doi.org/10.3762/bjoc.11.76.
30. Nyakuma, B.B.; Wong, S.L.; Faizal, H.M.; et al. Carbon dioxide torrefaction of oil palm empty fruit bunches pellets: Characterisation and optimisation by response surface methodology. *Biomass Convers. Biorefinery* **2022**, *12*, 5881–5900. https://doi.org/10.1007/s13399-020-01071-8.
31. Cho, D.-W.; Cho, S.-H.; Song, H.; et al. Carbon dioxide assisted sustainability enhancement of pyrolysis of waste biomass: A case study with spent coffee ground. *Bioresour. Technol.* **2015**, *189*, 1–6. https://doi.org/10.1016/j.biortech.2015.04.002
32. Kim, J.; Lee, J.; Kim, K.-H.; et al. Pyrolysis of wastes generated through saccharification of oak tree by using CO2 as reaction medium. *Appl. Therm. Eng.* **2017**, *110*, 335–345. https://doi.org/10.1016/j.applthermaleng.2016.08.200.
33. Guizani, C.; Escudero Sanz, F.J.; Salvador, S. Effects of CO_2 on biomass fast pyrolysis: Reaction rate, gas yields and char reactive properties. *Fuel* **2014**, *116*, 310–320. https://doi.org/10.1016/j.fuel.2013.07.101.
34. Chen, D.; Chen, F.; Cen, K.; et al. Upgrading rice husk via oxidative torrefaction: Characterization of solid, liquid, gaseous products and a comparison with non-oxidative torrefaction. *Fuel* **2020**, *275*, 117936. https://doi.org/10.1016/j.fuel.2020.117936.
35. Dutta, S.; Bhat, N.S. Catalytic Transformation of Biomass-Derived Furfurals to Cyclopentanones and Their Derivatives: A Review. *ACS Omega* **2021**, *6*, 35145–35172. https://doi.org/10.1021/acsomega.1c05861.
36. Jung, D.; Duman, G.; Zimmermann, M.; et al. Hydrothermal carbonization of fructose—Effect of salts and reactor stirring on the growth and formation of carbon spheres. *Biomass Convers. Biorefinery* **2023**, *13*, 6281–6297. https://doi.org/10.1007/s13399-021-01782-6.
37. Niu, Q.; Du, X.; Li, K.; et al. Role of catalyst porosity and acidity in nitrogen transformation during catalytic fast pyrolysis of microalgae: Study on extracted protein and model amino acids. *Energy Convers. Manag.* **2024**, *322*, 119210. https://doi.org/10.1016/j.enconman.2024.119210.
38. Nsibi, C.; Pozzobon, V.; Escudero-Sanz, J.; et al. Catalytic Effects of Potassium Concentration on Steam Gasification of Biofuels Blended from Olive Mill Solid Wastes and Pine Sawdust for a Sustainable Energy of Syngas. *Sustainability* **2024**, *16*, 9040.
39. Chen, W.-H.; Aniza, R. Specific chemical bioexergy and microwave-assisted torrefaction optimization via statistical and artificial intelligence approaches. *Fuel* **2023**, *333*, 126524. https://doi.org/10.1016/j.fuel.2022.126524.
40. Md Salim, R.; Asik, J.; Sarjadi, M.S. Chemical functional groups of extractives, cellulose and lignin extracted from native Leucaena leucocephala bark. *Wood Sci. Technol.* **2021**, *55*, 295–313. https://doi.org/10.1007/s00226-020-01258-2.
41. Liu, Y.; Rokni, E.; Yang, R.; et al. Torrefaction of corn straw in oxygen and carbon dioxide containing gases: Mass/energy yields and evolution of gaseous species. *Fuel* **2021**, *285*, 119044. https://doi.org/10.1016/j.fuel.2020.119044.
42. Shahbeik, H.; Kazemi Shariat Panahi, H.; Dehhaghi, M.; et al. Biomass to biofuels using hydrothermal liquefaction: A comprehensive review. *Renew. Sustain. Energy Rev.* **2024**, *189*, 113976. https://doi.org/10.1016/j.rser.2023.113976.
43. Basu, P. Chapter 7—Gasification Theory. In *Biomass Gasification, Pyrolysis and Torrefaction*, 3rd ed.; Basu, P., Ed.; Academic Press: Cambridge, MA, USA, 2018; pp. 211–262.
44. Eseltine, D.; Thanapal, S.S.; Annamalai, K.; et al. Torrefaction of woody biomass (Juniper and Mesquite) using inert and non-inert gases. *Fuel* **2013**, *113*, 379–388
45. Uemura, Y.; Saadon, S.; Osman, N.; et al. Torrefaction of oil palm kernel shell in the presence of oxygen and carbon dioxide. *Fuel* **2015**, *144*, 171–179. https://doi.org/10.1016/j.fuel.2014.12.050.
46. Cho, D.-W.; Lee, J.; Yoon, K.; et al. Pyrolysis of $FeCl_3$-pretreated spent coffee grounds using CO_2 as a reaction medium. *Energy Convers. Manag.* **2016**, *127*, 437–442. https://doi.org/10.1016/j.enconman.2016.09.036.

47. Quan, C.; Zhou, Y.; Gao, N.; et al. Direct CO_2 capture from air using char from pyrolysis of digestate solid. *Biomass Bioenergy* **2023**, *175*, 106891. https://doi.org/10.1016/j.biombioe.2023.106891.
48. Sun, Y.; Dong, B.; Wang, L.; et al. Technology selection for capturing CO_2 from wood pyrolysis. *Energy Convers. Manag.* **2022**, *266*, 115835. https://doi.org/10.1016/j.enconman.2022.115835.
49. Wang, T.; Hsu, C.-L.; Huang, C.-H.; et al. Environmental impact of CO_2-expanded fluid extraction technique in microalgae oil acquisition. *J. Clean. Prod.* **2016**, *137*, 813–820. https://doi.org/10.1016/j.jclepro.2016.07.179.
50. Aho, A.; DeMartini, N.; Pranovich, A.; et al. Pyrolysis of pine and gasification of pine chars—Influence of organically bound metals. *Bioresour. Technol.* **2013**, *128*, 22–29. https://doi.org/10.1016/j.biortech.2012.10.093.
51. Frost, D.L.; Goroshin, S.; Levine, J.; et al. Critical Conditions for Ignition of Aluminum Particles in Cylindrical Explosive Charges. *AIP Conf. Proc.* **2006**, *845*, 972–975. https://doi.org/10.1063/1.2263484.
52. Barabulica, I.; Secula, M.S.; Asoltanei, A.M.; et al. Experimental Study on the Reaction of Magnesium in Carbon Dioxide and Nitrogen Atmosphere. *ChemEngineering* **2024**, *8*, 41.
53. Zhang, S.; Wang, J.; Zhu, S.; et al. Effects of $MgCl_2$ and $Mg(NO_3)_2$ loading on catalytic pyrolysis of sawdust for bio-oil and MgO-impregnated biochar production. *J. Anal. Appl. Pyrolysis* **2020**, *152*, 104962. https://doi.org/10.1016/j.jaap.2020.104962.
54. Aniza, R.; Chen, W.-H.; Lin, Y.-Y.; et al. Independent parallel pyrolysis kinetics of extracted proteins and lipids as well as model carbohydrates in microalgae. *Appl. Energy* **2021**, *300*, 117372. https://doi.org/10.1016/j.apenergy.2021.117372.
55. Chen, R.; Zhang, S.; Cong, K.; et al. Insight into synergistic effects of biomass-polypropylene co-pyrolysis using representative biomass constituents. *Bioresour. Technol.* **2020**, *307*, 123243. https://doi.org/10.1016/j.biortech.2020.123243.
56. Menéndez, J.A.; Arenillas, A.; Fidalgo, B.; et al. Microwave heating processes involving carbon materials. *Fuel Process. Technol.* **2010**, *91*, 1–8. https://doi.org/10.1016/j.fuproc.2009.08.021.
57. Dupont, C.; Boissonnet, G.; Seiler, J.-M.; et al. Study about the kinetic processes of biomass steam gasification. *Fuel* **2007**, *86*, 32–40. https://doi.org/10.1016/j.fuel.2006.06.011.
58. Kawamoto, H. Review of reactions and molecular mechanisms in cellulose pyrolysis. *Curr. Org. Chem.* **2016**, *20*, 2444–2457.